NASA/TM–20250008757

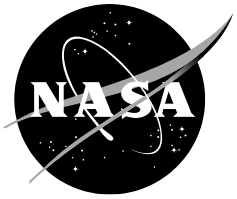

The Integration of eVTOL Aircraft and Infrastructure into San Jose Mineta International Airport

** All authors contributed equally to this memo. The names are listed alphabetically by surname.*

Skylar Bogner
Woodinville High School, Woodinville, WA

Pranav Karthikeyan
Montgomery High School, Skillman, NJ

Ganesh Ramamurthi
Richard Montgomery High School, Potomac, MD

Krish Saini
West Windsor Plainsboro High School North, Plainsboro, NJ

Lousia Regulla-Wilkens
Sevenoaks School, London, UK

Elliana Zhao
International School, Bellevue, WA

August 2025

NASA STI Program Report Series

The NASA STI Program collects, organizes, provides for archiving, and disseminates NASA's STI. The NASA STI program provides access to the NTRS Registered and its public interface, the NASA Technical Reports Server, thus providing one of the largest collections of aeronautical and space science STI in the world. Results are published in both non-NASA channels and by NASA in the NASA STI Report Series, which includes the following report types:

- TECHNICAL PUBLICATION. Reports of completed research or a major significant phase of research that present the results of NASA Programs and include extensive data or theoretical analysis. Includes compilations of significant scientific and technical data and information deemed to be of continuing reference value. NASA counterpart of peer-reviewed formal professional papers but has less stringent limitations on manuscript length and extent of graphic presentations.

- TECHNICAL MEMORANDUM. Scientific and technical findings that are preliminary or of specialized interest, e.g., quick release reports, working papers, and bibliographies that contain minimal annotation. Does not contain extensive analysis.

- CONTRACTOR REPORT. Scientific and technical findings by NASA-sponsored contractors and grantees.

- CONFERENCE PUBLICATION. Collected papers from scientific and technical conferences, symposia, seminars, or other meetings sponsored or co-sponsored by NASA.

- SPECIAL PUBLICATION. Scientific, technical, or historical information from NASA programs, projects, and missions, often concerned with subjects having substantial public interest.

- TECHNICAL TRANSLATION. English-language translations of foreign scientific and technical material pertinent to NASA's mission.

Specialized services also include organizing and publishing research results, distributing specialized research announcements and feeds, providing information desk and personal search support, and enabling data exchange services.

For more information about the NASA STI program, see the following:

- Access the NASA STI program home page at http://www.sti.nasa.gov

- Help desk contact information:

https://www.sti.nasa.gov/sti-contact-form/ and select the "General" help request type.

NASA/TM–20250008757

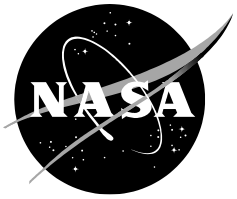

The Integration of eVTOL Aircraft and Infrastructure into San Jose Mineta International Airport

** All authors contributed equally to this memo. The names are listed alphabetically by surname.*

Skylar Bogner
Woodinville High School, Woodinville, WA

Pranav Karthikeyan
Montgomery High School, Skillman, NJ

Ganesh Ramamurthi
Richard Montgomery High School, Potomac, MD

Krish Saini
West Windsor Plainsboro High School North, Plainsboro, NJ

Lousia Regulla-Wilkens
Sevenoaks School, London, UK

Elliana Zhao
International School, Bellevue, WA

National Aeronautics and
Space Administration

Ames Research Center
Mountain View, CA

August 2025

The Integration of eVTOL Aircraft and Infrastructure into San Jose Mineta International Airport

Skylar Bogner, Pranav Karthikeyan, Ganesh Ramamurthi,
Krish Saini, Louisa Regulla-Wilkens, Elliana Zhao

August 2025

Contents

Acknowledgments

The authors would like to acknowledge Milad Memarzadeh and Swati Saxena for their excellent guidance and support throughout this study as our mentors. The authors would also like to thank Shannon Zelinski and everyone at the NASA Ames Research Center who made this experience possible, as well as all the AMES Research Center employees who gave us a tour of the facilities.

Abstract

With the average American spending around 43 hours a year sitting in traffic[1], and automobile emissions in the US accounting for 57% of all transportation emissions[2], traditional transportation infrastructure can no longer keep pace with growing demand and environmental concerns. Electric vertical take-off and landing vehicles (eVTOLs) offer an environmentally friendly approach to efficiently transporting individuals while reducing stress on current infrastructure. As many companies work towards effectively integrating eVTOLs, or air taxis, into urban environments, airports have become the most likely candidates for housing early air taxi hubs. However, limited physical space at airports, the complexity of coordinating with existing air traffic, noise concerns, weather challenges, and additional constraints stand in the way of successfully implementing this technology. The present study develops a geospatial data-driven approach using Python-based spatial analysis and A* pathfinding algorithms to identify optimal vertiport locations in airports and seamlessly integrate them into the air traffic at a chosen location. The analysis covered flight traffic density under 3,000 feet, wind favorability, proximity to terminals, access to frequent destinations, and dynamic no-fly zones of the San Jose Mineta International Airport (SJC). The data was used to generate colored heatmaps that revealed the most suitable vertiport sites and highlighted airspace congestion. This approach also produced snapshots across different daily intervals, enabling algorithmically optimized flight path planning for eVTOL operations based on the time of day. Potential vertiport locations were tested to find the best configuration of landing pads and gates tolerating the highest throughput of air taxis. Further investigation revealed two optimal vertiport locations concentrated in a 4-mile area of SJC, with peak operational windows occurring during 12-2 PM PST when traffic and wind conditions align favorably. These findings provide a systematic foundation for integrating eVTOLs and other Advanced Air Mobility (AAM) into existing airport infrastructure, with a system offering a replicable framework applicable to airports worldwide.

1 Introduction

The case for air taxis is compelling; however, integrating them into existing infrastructure is challenging. The air mobility market is estimated to be worth $4.59 billion in 2024 and projected to reach $23.47 billion by 2030.[3] This represents a compound annual growth rate (CAGR) of 31.2%. This level of growth and economic value is a driving force for the development of eVTOLs (electric vertical takeoff and landing), as evidenced by the 1000 new eVTOL[4] designs created by companies around the world. Plans have been developed to integrate eVTOLs into major city centers, but the current focus is shifting to add them to airports. Integrating eVTOLs effectively into an airport would allow people to avoid heavy congestion and would significantly reduce commute time, saving anywhere from 23 minutes for short commutes (50km) to 76 minutes for regional commutes (300km).[5] Additionally, the heavy congestion on roads, which has resulted in people experiencing over 102 hours of traffic[6], would be reduced by the introduction of air taxis. Air taxis are more efficient and sustainable, as they are 100% electric, resulting in a significant decrease in greenhouse gas emissions.[7] Therefore, this developing technology is causing airports to face increasing pressure to adapt and design new infrastructure to efficiently integrate the new eVTOLs.

With almost 20,000 public and private airports in the USA and over 21,000 commercial flights landing and taking off in the USA per day[8], integrating the needed infrastructure and flight paths for eVTOLs will be arduous. These challenges arise from the different layouts and available resources at each airport, as well as the specific requirements and regulations pertaining to eVTOLs. Most US airports operate at near capacity, making it very difficult to integrate eVTOLs as the airports lack the space for appropriate takeoff and landing infrastructure.[10]

Vertiports are infrastructure designed for the vertical take-off and landing of aircraft.[11] They require large areas as the landing zones need to be 3 times the diameter, with passenger pick-up and drop-off areas required by the FAA.[12] The vertiports would also require additional frameworks, such as charging stations, as a 1.5MW charger is required to provide 300kWh in under 15 minutes to the eVTOLs[13], so that they can be efficient and maximize daily flight frequency.

Furthermore, airports have several restricted zones within and/or surrounding them, reducing the available area even further. These restrictions are to ensure safety, prevent acts of terrorism and unlawful interference with aircraft operations, as well as to provide many other considerations.[14] This means extensive planning would be required to integrate the eVTOLs, as there is a risk of disrupting existing operations while being expensive to deploy and operate.[15]

eVTOLs operate at around 2,000 feet, which poses other challenges, as there are airspace restrictions to prevent collisions with aircraft. They are likely to interfere with current operations and put more pressure on the current ATCOs (air traffic controllers) who are already experiencing shortages.[16] Airports are already struggling to manage coordination between the airlines, general aviation, and military operations. Many also have the goal to increase the number of flights going through the airport further[16], so the addition of eVTOLs would only exceed the traffic controller capacity.[17] This would lead to the airport having to decide whether to honor its long-standing relationships with airline partners or to prioritize new eVTOL technology.[17]

These are only a few of the many variables that need to be considered by airports before integrating air taxis. Others, including noise, sustainability, and visual pollution, must be considered as eVTOLs would need to be added in a way that results in minimal impact.[15]

The current aviation industry is predicated on highly structured and centralized air traffic control systems, which are designed for commercial airlines and large airports. The integration of eVTOLs would require redesigning to create an aviation environment based on a more unpredictable and dynamic model.[15]

This study will focus on how to incorporate air taxis efficiently into the San Jose Mineta International Airport (SJC) through two lenses: finding ideal locations for vertiport placement and integrating air taxi traffic into existing airplane traffic. Through multidimensional analysis, we have determined the most suitable locations and schedules for air taxis, allowing for seamless integration into existing airports. Over the course of this paper, we aim to cover the entire process of implementing eVTOL infrastructure into current aviation environments, providing a replicable foundation for future projects in this field.

2 Related Works

Before building our models, it was important to look at ongoing research and advancements in this space.

Shannon Zelinski's paper[18] explores three topologies, each designed around four Touchdown and Lift-Off (TLOF) Areas at the corners of a square-shaped vertiport. These topologies are made of vertiport pads, vertiport parking, and major and minor taxiways. When the topologies are tested for space efficiency and throughput, factors including wind direction that inhibit the use of specific TLOFs as arrival or departure pads and taxiing time from the TLOFs to the vertiport parking spaces are considered. Dr. Zelinski's research is similar to this paper, as this study also explores different configurations in a rectangular shape, but focuses on real locations and designing topographies that fit within these areas.

Kapil S. Sheth's paper[19] explores creating composite suitability maps, breaking them up into different cells, and scoring the cells based on their suitability. The study also created optimal flight paths between origin and destination for eVTOLs, and analyzed the suitability of those flight paths. We used a similar technique as we explored using the heat maps for an airport and creating a score based system to analyze the different possible areas. After choosing different sites, we created possible flight paths to key destinations around the airport. To build upon this research, we looked into the different configurations of the vertiports when possible vertiport locations were found.

Feldhoff and Roque's case study[21] explored vertiport infrastructure requirements for air taxi operations at Cologne Bonn Airport. They investigated demand modelling, plausible aircraft configurations, and integration with existing airport structures. Knowing the demand and making assumptions, they estimated that one FATO (Final Approach and Takeoff Area) would require 4-9 stands and used the vertiport measurements to identify possible locations. Then, they created a 'location selection criteria' list, which included passenger accessibility, obstacle clearance, noise impact, expandability, applicability, and the availability of each site. We implemented a similar system into our method, as different areas were judged on several factors. As in the Cologne Bonn analysis, our model considers proximity to terminals, operational safety places (such as proximity to runways), and the adaptability of existing infrastructure. However, our methodology introduces several advancements to address the unique complexity and demands of integrating eVTOL operations into dense, high-traffic environments like SJC. We designed a data-driven heat map approach to help visualize and show where the best spot to place vertiports in the airport is. Feldhoff and Roques' framework shows high-level screening and feasibility assessment; our work adds on, showing operational planning and optimization by using real

data.

The paper by Di Mascio et al.[22] provides an in-depth overview of the emerging field of vertiports and discusses their role in making AAM possible. The review looks at the technical design, regulations, and how vertiports should fit into existing transportation networks, but mainly focuses on broad, high-level strategies and challenges. Our paper refines this by taking those general principles and putting them into practice at SJC using real-world data. We improve upon their work by using a scoring approach and evaluating the best locations to put the vertiports. Di Mascio and our paper bridge the gap between theory and application, offering a step-by-step methodology that can be used to guide actual vertiport placement and design.

In another paper, Lee and Cho[23] propose a three-stage geospatial analysis framework for locating optimal vertiport locations in a complex urban environment. Their approach includes suitability analysis, where they score areas based on factors like population density, land mix, traffic, and access to transport; regulation analysis, which removes any areas due to legal or safety reasons; and location allocation, which chooses the final sites considering city plans, land prices, and local demand. They tested this approach in two different places in South Korea, Busan and Jeju. Our study complements and extends Lee and Cho's framework by moving from a planned focus analysis to a more detailed site-specific application.

A recent study by Yoon et al.[24] in 2025 looks at how to choose vertiport locations by connecting them with major highways around Seoul, aiming to make UAM more useful for people who live or work outside city centers. The researchers use real travel and location data to score over a hundred possible spots, narrowing them down to the best places based on how well they link with busy roads and the level of travel demand nearby. Their study shows that putting vertiports near important buildings can improve access and make UAM services more efficient. This approach is similar to our study, but focuses more on the connections across the whole region rather than just one airport. Their study helped to support that combining detailed site analysis with a bigger picture network plan leads to better vertiport placement and more efficient UAM systems. Overall, these papers provided insight and tools that aided the development of our approach, inspiring us to apply this study design to San Jose International Airport.

3 Methods

3.1 General Vertiport Location

3.1.1 Airport Selection

Before beginning research into the integration of eVTOLs into the current infrastructure, it was crucial to establish the airport for this case study. Several aspects, such as weather, runway configuration, passenger demand, physical location, and other factors, need to be accounted for when selecting an airport. San Jose Mineta International Airport (SJC) experiences rather favorable weather conditions when it comes to precipitation, visibility, and temperature year-round.[25] SJC is also located at an elevation of just 62 ft ($\approx 19m$) above sea level[26], with surrounding terrain being relatively flat throughout the Santa Clara Valley—significantly easing approach and departure flight profiles and reducing mountainous turbulence risks.

Additionally, the airport's simple parallel runway design yielded two possible configurations, allowing us to easily map the flow of traffic without concern for various changes in runway configurations throughout our report. According to FAA documentation, SJC operates under Class C airspace during tower hours (generally 0600–0000 local). It lies under San Francisco Class B airspace, but is less restrictive than B-class environments, making air traffic routing simpler.[28]

Aside from the physical characteristics of the airport itself, San Jose is located in Silicon Valley, a populous location where there are large commutes between the towns and cities in the area.[30] Therefore, the demand for air taxis in this region will be large, and the possible destinations from SJC by air taxi are vast. Also, the airport's proximity to numerous tech companies such as Joby Aviation and Archer can hasten the implementation of eVTOLs into airports. Looking at transportation data from SJC, the airport experiences less congestion compared to its peers, with lower delay rates and cancellations, meaning that airport infrastructure will not be burdened by the integration of air taxis.

3.1.2 Vertiport Location Heat Map

To determine the coloring for the vertiport placement heatmap, we developed a multivariable scoring system that depicted suitable vertiport locations near SJC. While scoring, we examined each pixel's proximity to certain airport infrastructure, access to points of interest, location in restricted areas, and favorability to prevailing wind. Based on each of these factors, every pixel was given a composite score and colored accordingly on the grid. In the subsequent sections, the scoring procedure for each of the factors will be discussed in great detail.

3.1.2.1 Proximity to Important Locations

There are two very important factors to consider for the placement of a vertiport: proximity to the runway, and proximity to the terminals. The proximity to the runways will determine how independently air taxis can take off and land from runway operations. To be in accordance with the FAA's Recommended Minimum Distance, the vertiport FATO must be at least 500ft for small (12,500 lbs or less) or large airplanes (12,501 - 300,000 lbs) and 700ft for heavy airplanes (over 300,000 lbs).[11] SJC handles cargo and heavy commercial planes, so in order to be a safe distance from aircraft year-round, the vertiport FATO must be a minimum distance of 700ft from runways, where anything from 0-500ft from the runways is off limits entirely. For independent operations, the vertiport must be placed at least 2500ft from runways, which we selected as our ideal distance.[11]

For the chosen vertiport designs, passengers board and depart the eVTOL near or on the landing zones; therefore, the distance from the landing zones to the passengers' final destination must be taken into account. For this study, we have assumed all passengers will travel between the terminals and the vertiport, excluding other airport facilities. We have chosen Terminal B as the target location since it is the larger of the two terminals and handles both domestic and international flights.

The distances to the runways and terminal B are calculated separately and then combined and normalized to produce one final score. To find the location of the runways in Figure 1, we perform a Probabilistic Hough Line Transform of a black and white image. The green lines in the following image mark the detected runways.

Figure 1: Runways of SJC
Imagery ©2024 Google, Vexcel Imaging US, Inc. Imagery dates: 11 Mar. 2022–18 July 2024.

After finding the location of the runways, the runways are converted to vectors and subtracted from a meshgrid of pixel coordinates to find the vectors from the start of each line to a pixel. We then perform a scalar projection of the point vectors onto the runway vectors and clip the result to the length of the line segment. Finally, we calculate the coordinate of the closest point on the line and calculate the Euclidean distance from each pixel to the closest point on both runways. The minimum of the two distances is taken as the final proximity to the runway. The maximum deviation from the ideal distance (2500ft) is then calculated and used to perform deviation-based normalization on the

runway distance data. For the final proximity score, the Euclidean distance between the pixels and a chosen point at terminal B is calculated, added to the runway distances, and normalized.

3.1.2.2 Restricted Zones

The only restricted zone accounted for within a 3.2 km radius of the SJC runways is within 500ft of the runway.[11] In our heatmaps (Figure 21), we marked this with a dark red, indicating it was off limits as a potential location. After calculating all scores for each pixel, the final array is compared to a boolean mask of runway distances that are less than 500ft (inclusive); any points that match the mask are assigned the dark red color.

3.1.2.3 Access to Points Of Interest

We analyzed possible air taxi destinations and chose 11 that would have the greatest demand: San Francisco, San Francisco Airport (SFO), Oakland, Oakland Airport (OAK), San Jose, Mountain View, Cupertino, Sunnyvale, Santa Clara, Palo Alto, and Fremont. To simplify the calculations for access to points of interest, we assumed a straight path from a pixel to each Point of Interest. The flight traffic line from the eVTOL air traffic map was plotted onto the vertiport location map to ensure the straight paths would not impede current airport operations.

To determine if a straight path crosses the flight path trend line, we performed a counterclockwise test on the trend line endpoints, pixels, and points of interest. This test returned True if point c was to the left of points a and b according to the following formula:

$$(c_y - a_y)\,(b_x - a_x) > (b_y - a_y)\,(c_x - a_x) \tag{1}$$

4 sets of points were tested for all pixels and points of interest in the form $(a_x, a_y, b_x, b_y, c_x, c_y)$:

$$\begin{aligned} \left(x_1^{\text{fl}}, y_1^{\text{fl}}, x^{\text{px}}, y^{\text{px}}, x^{\text{poi}}, y^{\text{poi}}\right) \\ \left(x_2^{\text{fl}}, y_2^{\text{fl}}, x^{\text{px}}, y^{\text{px}}, x^{\text{poi}}, y^{\text{poi}}\right) \\ \left(x_1^{\text{fl}}, y_1^{\text{fl}}, x_2^{\text{fl}}, y_2^{\text{fl}}, x^{\text{px}}, y^{\text{px}}\right) \\ \left(x_1^{\text{fl}}, y_1^{\text{fl}}, x_2^{\text{fl}}, y_2^{\text{fl}}, x^{\text{poi}}, y^{\text{poi}}\right) \end{aligned} \tag{2}$$

where **fl** stands for flight line, **px** stands for pixel, and **poi** stands for point of interest.

The results of the tests were then compared to determine whether the pixel and the off-screen point lie on opposite sides of the flight path trend line. If they do, the path is blocked, and the point is deemed unreachable for the pixel. From top to bottom, the above tests are labeled ccw_1, ccw_2, ccw_3, ccw_4.

$$(ccw_1 \neq ccw_2) \wedge (ccw_3 \neq ccw_4) \tag{3}$$

For each pixel, the total number of points of interest that can be reached without crossing the flight path trend line is aggregated and normalized.

3.1.2.4 Wind Favorability

Wind speed and direction data were sourced from the National Renewable Energy Laboratory (NREL), specifically from the Wind Integration National Dataset (WIND) Toolkit, which provides high-resolution modeled meteorological data at multiple heights above ground level from 2020. The data used in this study were obtained from an altitude of 10 meters, which closely approximates typical take-off and landing heights for air taxis. To download the data, we used the AWS Command Line Interface (CLI) to access NREL's public S3 bucket. The relevant wind files were then filtered by proximity to the California Bay Area and converted into standard CSV files. Any data points that were missing for each row were omitted. Wind data was obtained for every 1-1.5 miles or every hundredth of a degree latitude/longitude. Once the data were obtained, we designed a spatial wind model that penalized pixels that were in areas with suboptimal(opposing winds with strong speeds) wind speed and direction. In the dataset, wind speeds (S_{wind}) and directions (θ_{wind}) are provided at discrete geographic points. To assign wind conditions to each pixel in the grid, we applied bilinear spatial interpolation for wind speed and direction,

$$s_{\text{interp}}(x,y) = \sum_{i \in T(x,y)} \lambda_i(x,y) \cdot s_i \tag{4}$$

$$\theta_{\text{interp}}(x,y) = \sum_{i \in T(x,y)} \lambda_i(x,y) \cdot \theta_i \tag{5}$$

where the formula shows the interpolation for scalar field s and vector field θ at position (x, y) using barycentric coordinates λ_i over triangultion $T(x, y)$. This approach yields an interpolated wind vector for every pixel on our grid. Then, the angle of the path to a POI is calculated as shown:

$$\alpha_{\text{path}} = \arctan 2(y_{\text{poi}} - y, x_{\text{poi}} - x) \times \frac{180}{\pi} \tag{6}$$

Here, the length from a pixel to each POI is calculated in terms of the x and y direction, put into an inverse trigonometric function, and converted to degrees. Then, both the interpolated angle and α_{path} are converted to a value between 0 and 360 before calculating the angle difference according to the equation below.

$$\Delta\alpha = |\theta_{\text{wind}} - \alpha_{\text{norm}}| \tag{7}$$

Then, we obtain the smallest reference angle of α before calculating the Alignment Factor(A_{factor}) in the equation shown below.

$$A_{\text{factor}} = |\sin(\Delta\alpha)| + \max(0, -\cos(\Delta\alpha)) \times 0.3 \tag{8}$$

This formulation penalizes crosswinds (via the sine term) and adds a penalty for strong headwinds (via the cosine term). Pure crosswinds (90°) yield a maximum score of 1, while pure tailwinds score closer to 0. Headwinds are penalized, but are multiplied by 0.3 as they are less dangerous for eVTOLs as they take off.[31] The negative sign in front of the cosine ensures tailwinds are not penalized. As shown, suboptimal wind conditions will result in higher scores closer to one. Once the Alignment factor is calculated, the wind speeds for each pixel are normalized. Once that is completed, the total wind penalty score for a Single pixel-to-POI path is then computed.

$$W_{\text{poi\_wind}} = s_{\text{norm}} \times A_{\text{factor}} \times M_{\text{valid}} \tag{9}$$

The M_{valid} term determines whether the calculation is valid or not, as it determines whether the flight path to a POI does not cross a no-fly zone. Thus, the value of M_{valid} can only be 0 or 1. This computation is repeated for all POIs, and the final wind penalty score per pixel is computed as the average over all valid POI paths.

For generating the heat map composed of the average wind at 1 PM, the same approach was conducted. The main difference was that, at the beginning, all wind data in the bounding box was grouped by unique coordinate. Then, all datapoints were filtered by time for 1 PM PST or PDT, depending on the month. Afterwards, wind speed and direction were averaged and plotted as normal on the heatmap.

3.1.2.5 Composite Score

Now that the three main calculations have been completed, each makes up a 33.33% weight of the composite score. This even weighting ensures that all components for a pixel's score are treated evenly, preventing any bias from occurring. These composite scores are assigned to a color gradient and are mapped accordingly in the final visualization.

3.2 Air Traffic Heat Map

In order to help determine ideal vertiport locations, as well as establish a routing system that would supplement the vertiports of choice, we came up with an approach to establish a large-scale air traffic map of San Jose. For this map, air traffic data was downloaded from OpenSky's Weekly 24 Hours of State Vector Data dataset. Several weekdays' worth of data, evenly spanning the first six months of 2022. The map encompassed an area of 285 square miles around SJC, with a 10-mile radius to the East and West, and a 7-mile radius to the North and South. These measurements were chosen as they

approximate the radius that air traffic control towers cover in their operations.[32] To render the map, the latitude and longitude bounds of the image were defined, as well as a maximum altitude of 915 meters (3,000ft). This maximum altitude was chosen because the maximum height of air taxi operations was 2,000ft, and FAA regulations dictate that air taxis must be at least 1,000 feet from airplanes.[11] Next, the map was divided into a number of cells, with spatial resolution under the control of the operator. For this project, a 30 by 30 cell grid was used as it accurately captured aircraft while displaying data cleanly. Aircraft latitude and longitude data were then taken from the OpenSky dataset to map aircraft within the grid if they are within image bounds and fit the altitude limit. To place the aircraft on the grid, the program normalizes the aircraft's latitude and longitude relative to the maximum and minimum latitudes and longitudes of the image. The two resulting normalized numbers, one for latitude and one for longitude, can be interpreted as how far along each edge of the map the aircraft is. These numbers are then multiplied by the number of rows and columns, respectively, then floored. This provides the row and column that the aircraft falls under. This approach is an approximation, as it does not account for the curvature of the Earth. However, we calculated the maximum error at the boundaries of the grid to be 1.34 inches, which we deemed acceptable for this study.

For every plane in a cell, the cell's raw score increases by 1. After all cell scores are tallied, these scores are then normalized to be between 0 and 1. This allows the scores to be consistent regardless of the amount of data used, as the maximum score and minimum score will always be 1 and 0. Once normalized, the scores are mapped onto the image using a $\log_{10}$ gradient of transparent, to yellow, to orange, to red. This scale was chosen because in certain high-traffic areas, such as the runway, raw traffic increases exponentially compared to other locations. Therefore, plotting the data with a log scale allows cells with relatively low traffic, but still a significant amount of traffic for our purposes, to be seen.

This process was repeated five times: once for only the first 6 hours of every day, once for the second 6 hours, once for the third 6 hours, once for the fourth 6 hours, and lastly, once for all 24 hours of every day. This produced 5 heat maps that showed general air traffic patterns at different times. We also created additional maps with different conditions, such as air traffic on the weekends and the upper 5% days with the most traffic, to visualize whether the trends we observed on the weekdays persisted under different conditions. Each map had scores normalized relative to the data used in making that map. For example, normalization for the map for the first 6 hours of the day normalized scores including only traffic data for the first 6 hours.

3.3 Vertiport Location Selection

3.3.1 Possible Locations

3.3.1.1 Zoning

Referencing the SJC zoning map[28] and the FAA regulations on vertiport design[11], we found strict regulations regarding zoning for different parts of an airport. Identifying no-fly zones and important buildings in SJC was a crucial first step for narrowing down possible locations.

3.3.1.2 Types of Buildings/Areas

From the zoning information, we decided parking garages and airplane hangars were the only places vertiports could be placed. We considered the airport terminals, but realized that the terminals likely could not withstand substantial additional weight, especially with the rounded and aesthetic design of SJC terminals. Additionally, it would be very disruptive to the many passengers going through the airport every day.

3.3.1.3 Parking Garages

For this factor, we assumed that any parking area nearby could be used. The parking lots were then narrowed down based on how full they were.[33] Lots with usually more than 60% of their capacity filled were not chosen. For one of the parking lots, Economy Lot 1 (generally 50-60% full), we only used around half the original area for throughput calculations. Satellite images aided us in visualizing the total capacity filled for each location, especially for places for which we did not have data.

3.3.1.4 Final Buildings/Areas

We limited our considerations to buildings/areas that were in the shape of a rectangle. For example,

there were a couple of triangular areas that we did not test. This allowed for ease of throughput calculations and higher throughputs.

Finally, we made sure that the locations we selected were optimal by checking with the vertiport location heat map and choosing places that were only in blue/green. The heat map takes into account proximity to the terminal and distance from the center of runways, so we did not specifically measure the distances to account for these two factors.

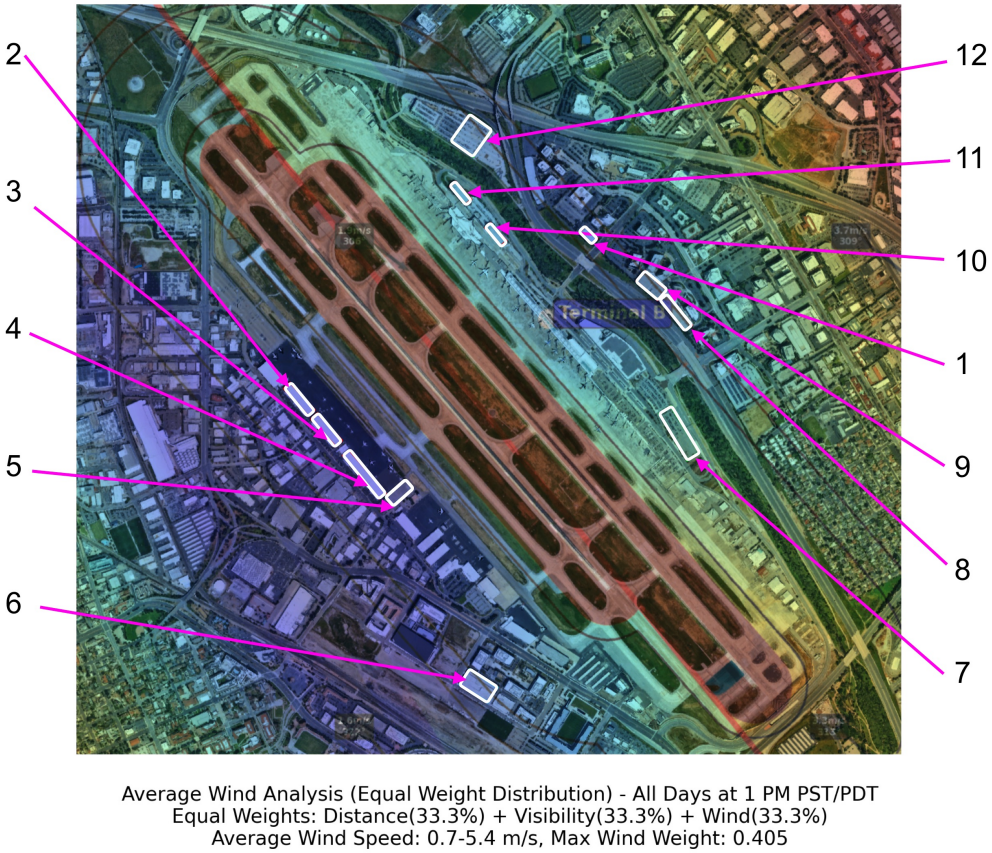

Figure 2: Initial 12 Locations
Imagery ©2024 Google, Vexcel Imaging US, Inc. Imagery dates: 11 Mar. 2022–18 July 2024.

In the end, we ended up with twelve locations. Most of these locations were parking garages in and around SJC. These locations are outlined in white and labeled Figure 2.

3.3.2 Topographies

This section of the paper was heavily influenced by Fedholff and Roque's paper[21] on integrating air taxis into the Cologne Bonn Airport, and Vázquez and Manuel's paper[34] on different vertiport topographies.

3.3.2.1 eVTOL Research

We chose Archer air taxis as our reference because it was recently approved to be the official 2028 Los Angeles Olympics air taxi provider. Los Angeles is close in proximity to San Jose, so the weather conditions are similar, and the Archer air taxis would be viable.

Archer Aviation created a two-seater electric vertical takeoff and landing (eVTOL) aircraft called Maker. It weighs around 3,300 pounds and is fully electric. Archer has shared that it has the goal of automating Maker, allowing it to be controlled by a screen at the front of the eVTOL. On December 1, 2022, it was published that Maker was able to reach speeds of around 91 Knots (105mph), which it

can sustain for approximately 60 miles.[39] It contains 12 propellers, which provide a vertical lift during take-off and landing.

The propulsion of the aircraft during forward flight is created by the forward 6 propellers, each equipped with 5 blades, which allow the aircraft to tilt forward into a cruise position. The remaining 6 propellers are exclusively used for the landing and take-off. The wings have a similar design and function to the wings on a conventional plane with a wing span of 40ft. The Maker is powered by a 75kWh Meru lithium-ion battery system, which only takes 10 minutes between flights to recharge. Archer estimates that one Maker taxi will be able to complete 40 flights per day at a cost of around $3-4 per person per mile.[8] Transporting people from San Francisco airport to San Jose will be cut down from 2 hours to just 17 minutes. The eVTOL cruises at a max altitude of around 2,000 feet and only produces 45dB of sound due to propellers spinning at low tip speed.

Archer has also been developing a new eVTOL called Midnight, which will fit 4 passengers and 1 pilot. While it shares many features with Maker, it is optimized for shorter distances of around 20-50 miles. It has a payload capacity of 1,000 pounds and would be well-suited for shuttles between airports and homes. It has 12 propellers and a wing span of around 48ft. The 6 batteries hold around 142kWh and support nearly 1,300 kW of power draw.[42]

3.3.2.2 Topography Design Components

Vertiport topographies are made up of three components: vertiport pads, gates, and taxiways. The specific topography design is important to give a vertiport location the highest throughput.

A vertiport pad is where an air taxi takes off and lands, a vertiport gate is where the air taxi goes to drop off and pick up passengers, and a vertiport taxiway is the specific road that an air taxi takes to go from the vertiport pad to the vertiport gate.

Assumptions

- Between Midnight & Maker, Midnight has a greater diameter (wingspan), so we designed the vertiports to accommodate that model
- Safety areas (SA) can extend in clear airspace - when a vertiport is on top of a building and next to the edge of the building, the safety area can be excluded in area calculations[11]
- Safety area for the gate and taxiway are 1.5 the diameter/wingspan of the eVTOL (D) - an assumption made due to lack of formal regulations on it

Vertiport Pad Element	Dimensions (Width/Length)
TLOF	D
FATO	2D
SA	3D

A TLOF is the touchdown and lift-off area, and the FATO is the final approach and takeoff area. The TLOF is often centered within the larger FATO area.

The vertiport pad dimensions are based on the 2022 FAA requirements, but updated 2024 FAA regulations have been released that allow the SA to be 2.5D instead of 3D.

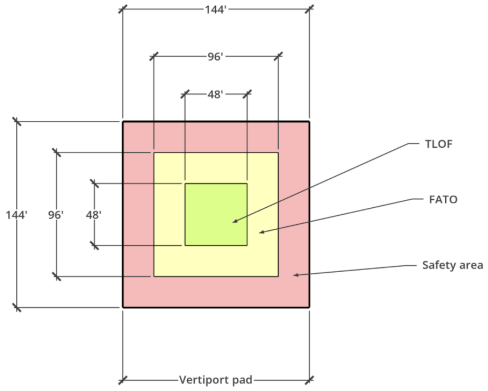

Figure 3: Vertiport Pad

Gate Element	Dimensions (Diameter)
Gate	D
SA	1.5D

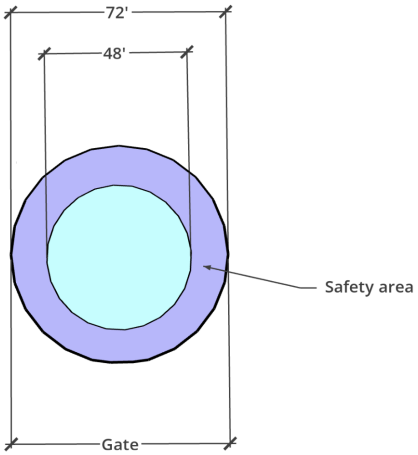

Figure 4: Vertiport Gate

Taxiway Element	Dimensions (Width)
Taxiway	D
SA	1.5D

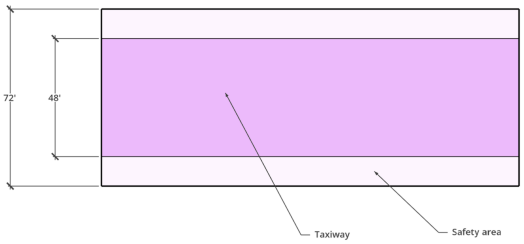

Figure 5: Vertiport Taxiway

3.3.2.3 Three Types Of Topographies

After designing different topographies with reference to other papers[34], we settled on 3 different topographies to test - Single, Linear, and Circuit. Other designs were deemed inefficient for the factors mentioned below. Our references are limited as we only had access to publicly available sources.

Criteria:

- All landing/take-off pads need edge access
- Space efficient - minimal empty space between the components and shortest possible taxiway lengths
- If a topography has a taxiway, there needs to be one taxiway to go from the landing pad to the gate, and one to go from the gate to the take-off pad. eVTOLs cannot interfere with each other

In our designs, vertiport pads can be placed right next to each other, as we do not consider flight paths entering and exiting vertiports.

The difference between these topographies is the number of gates and whether the take-off/landing pad is the same. The table below highlights this difference.

Topographies	Gates	Take-off/Landing Pad
Single	No Gates	Same Place
Linear	Gates	Same Place
Circuit	Gates	Separate Place

3.3.2.4 Single

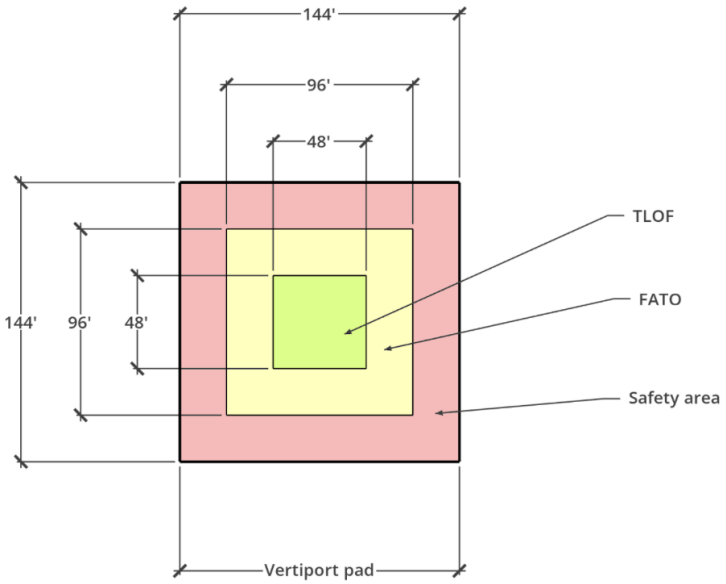

Figure 6: Single Topography With 1 Pad

The Single design was tested as a baseline, as it is the simplest topography. It is made up of a vertiport pad consisting of a TLOF, FATO, and safety area. It is the most compact, so it can potentially fit in small areas that other topographies cannot fit.

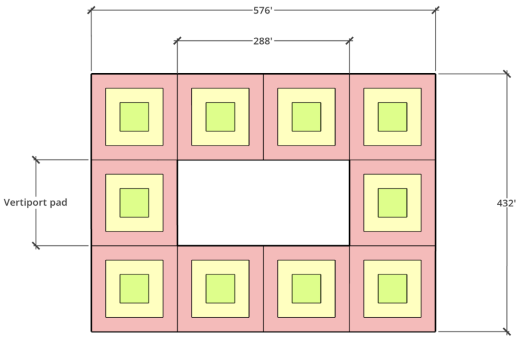

Figure 7: Single Topography With 8 Pads

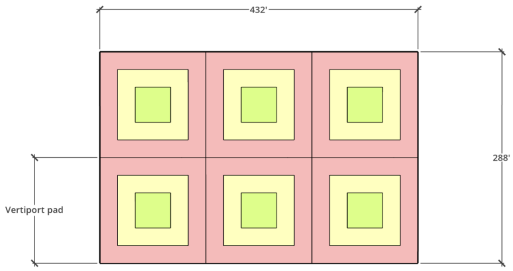

Figure 8: Single Topography With 6 Pads

Figure 8 shows one way the Single topography can expand. In smaller areas, there can only be a maximum of two rows of vertiport pads to prevent air taxis from flying over each other. If a given area is large enough, there can be additional vertiport pads lining the edges between the two rows, as shown in Figure 7.

3.3.2.5 Linear

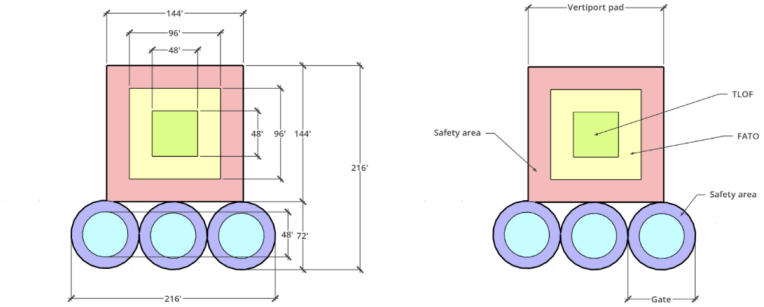

Figure 9: Linear Topography

Figure 9 shows the topography for Linear. This design was taken from the paper by Manuel. It consists of a vertiport pad and 2 to 3 gates, depending on the available space.[34] Figure 10 shows one way that this design can be expanded in larger areas. The placement of these modular vertiports in a larger area follows the same rules as Single.

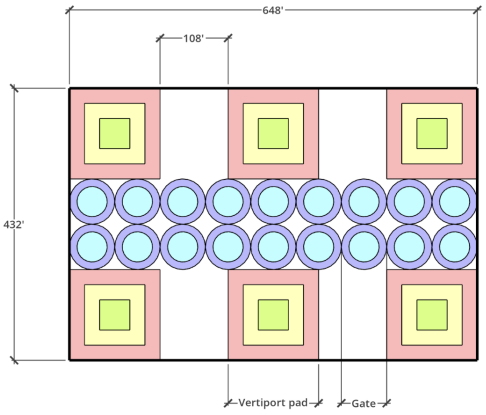

Figure 10: Linear Topography In Larger Areas

3.3.2.6 Circuit

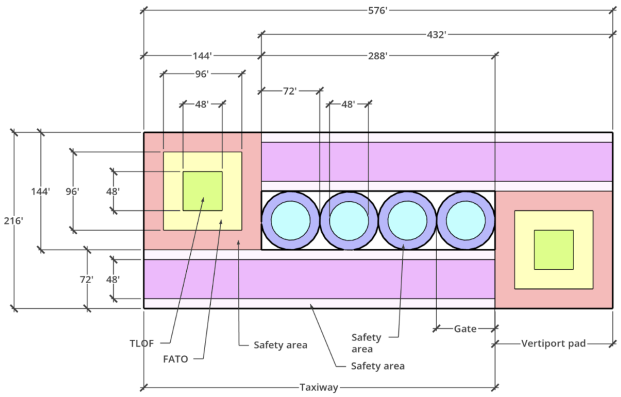

Figure 11: Circuit Topography

The Circuit topography consists of two vertiport pads, one for take-off and one for landing, two taxiways, and gates. The two taxiways prevent interference, as mentioned in the criteria for these designs. Interference on the taxiway would cause a delay. We were unsure how to calculate the cycle time with interference, so it was a major reason several other topographies with separate take-off/landing pads were not tested. Figure 12 shows one way the Circuit topography can be expanded into larger areas.

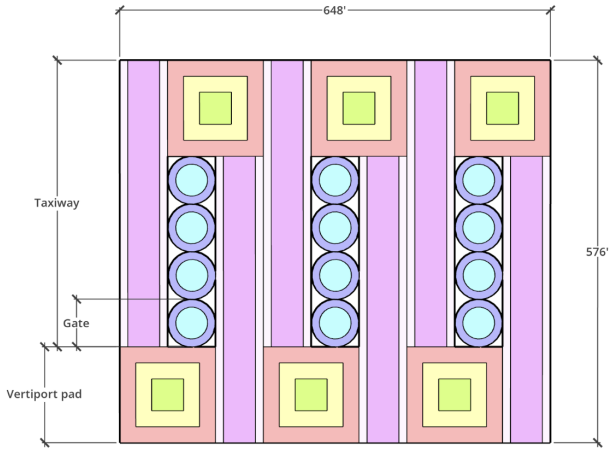

Figure 12: Circuit Topography In Larger Areas

3.3.3 Throughput Calculations

3.3.3.1 Cycle Time

The cycle time is the average time between air taxis leaving the vertiport or the time between flights for a particular topography. The gate2pad ratio is the number of gates there are for one vertiport pad. Finding the optimal cycle time helps us limit the number of gate2pad ratios we tested for the potential vertiport locations.

These cycle times do not take into account the travel time along taxiways, nor the time for charging. Airport space and infrastructure are limited[20], so we assumed it would not be logical to implement charging directly at the airport. Instead, these eVTOLs would charge at other vertiports around the city. The calculated times are under ideal conditions where there is no delay in any step of the process.

These cycle times are the cycle times after the first hour; the cycle times vary slightly at first, which is supported by the tables below.

Single The Single topography has no gates, so the cycle time is the sum of the landing, passenger boarding, and take-off time, which is $2 + 6 + 2 = 10$ minutes.

Linear The take-off and landing happen on the same vertiport pad, so an eVTOL must exit the vertiport and one must enter the vertiport for a cycle to be complete. The minimum cycle time for Linear must then be 4 minutes; 2 minutes to exit, and 2 minutes for another eVTOL to enter and fill the gate. This ensures the vertiport is operating at max capacity.

The first column of the table is the time, in minutes, from when the first air taxi enters the vertiport. The gate columns show the time an air taxi has spent at that gate. N/A means there are no eVTOLs at the gate. The "Time From Last Flight" column shows the time between one eVTOL leaving the vertiport and the last eVTOL leaving the vertiport, which is the time between flights. This value helps calculate the average cycle time.

Symbol	Meaning
N/A	None In Gate
0 (min)	Just Entered Gate
6 (min)	Ready To Leave
6+ (min)	Has Extra Wait Time
	Using Vertiport Pad
	Repeating Sequence
#	Final Cycle Time

Figure 13: Key for the Tables Below

Time	Gate 1	Gate 2	Time From Last Flight
0	0	N/A	
2	2	0	
4	4	2	
6	6	4	
8	N/A	6	
10	0	8	
12	2	N/A	4
14	4	0	
16	6	2	
18	N/A	4	6
20	0	6	
22	2	N/A	4
24	4	0	
26	6	2	
28	N/A	4	6
30	0	6	
32	2	N/A	4
34	4	0	
36	6	2	
			Cycle Time = (6 + 4)/2 = 5

Time	Gate 1	Gate 2	Gate 3	Time From Last Flight
0	0	N/A	N/A	
2	2	0	N/A	
4	4	2	0	
6	6	4	2	
8	N/A	6	4	
10	0	8	6	
12	2	N/A	8	4
14	4	0	10	
16	6	2	N/A	4
18	8	4	0	
20	N/A	6	2	4
22	0	8	4	
24	2	N/A	6	4
26	4	0	8	
28	6	2	N/A	4
30	8	4	0	
32	N/A	6	2	4
34	0	8	4	
36	2	N/A	6	4
38	4	0	8	
40	6	2	N/A	4
42	8	4	0	
44	N/A	6	2	4
46	0	8	4	
				Cycle Time = 4

Figure 14: Linear Cycle Times

Since one eVTOL must leave and one must enter, a green N/A is followed by a green 0, before the next eVTOL can leave. With this minimum cycle time in mind, the cycle time for a gate2pad ratio of 2 and 3 was calculated. The table on the left shows a ratio of 2, and the table on the right shows

a ratio of 3 (Figure 14). The cycle time for a gate2pad ratio of 3 already equaled the minimum cycle time, so no further gate2pad ratios were simulated. If any more gates were added, the cycle time would stay the same, while the wait time, or how much extra time an air taxi spends in the gate before it can take off, would increase by 4 minutes for every gate added.

Even though a gate2pad ratio of 2 had a longer cycle time, we still tested this topography due to its more compact design.

Circuit Figure 15 shows tables used to estimate cycle times using circuit topography gate2pad ratios, using the same key in Figure 13. Since the take-off and landing happen on separate vertiport pads, an eVTOL can exit and one can enter simultaneously. This is why there is no green N/A, and only green 0. The minimum cycle time is therefore only 2 minutes.

Time	Gate 1	Gate 2	Gate 3	Time From Last Flight
0	0	N/A	N/A	
2	2	0	N/A	
4	4	2	0	
6	6	4	2	
8	0	6	4	
10	2	0	6	2
12	4	2	0	2
14	6	4	2	
16	0	6	4	4
18	2	0	6	2
20	4	2	0	2
22	6	4	2	
24	0	6	4	4
26	2	0	6	2
28	4	2	0	2
30	6	4	2	
32	0	6	4	4
34	2	0	6	2
36	4	2	0	2
				Cycle Time = (4 + 2 + 2)/3 = 8/3

Time	Gate 1	Gate 2	Gate 3	Gate 4	Time From Last Flight
0	0	N/A	N/A	N/A	
2	2	0	N/A	N/A	
4	4	2	0	N/A	
6	6	4	2	0	
8	0	6	4	2	
10	2	0	6	4	2
12	4	2	0	6	2
14	6	4	2	0	2
16	0	6	4	2	2
18	2	0	6	4	2
20	4	2	0	6	2
22	6	4	2	0	2
24	0	6	4	2	2
26	2	0	6	4	2
28	4	2	0	6	2
30	6	4	2	0	2
32	0	6	4	2	2
34	2	0	6	4	2
36	4	2	0	6	2
					Cycle Time = 2

Figure 15: Circuit Cycle Times

The left table shows a gate2pad ratio of 3, and the right shows a ratio of 4 (Figure 15). The cycle time for a ratio of 4 was found to be the minimum cycle time, so no further gate2pad ratios were simulated.

A gate2pad ratio of 3 was not tested because the Circuit topography is not as modular as a Single. Having a separate landing and taking-off vertiport pad means the greatest gate2pad ratio would be a more efficient use of space.

3.3.3.2 Calculation Program

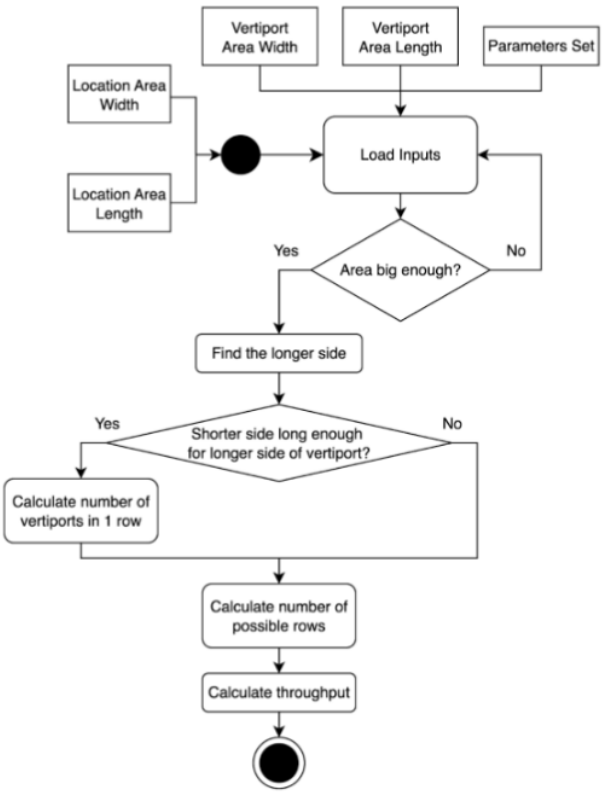

Figure 16: Flowchart for Throughput Calculations

Figure 16 shows the general idea of how the throughputs were calculated for all three topographies. The following table shows the parameters that we used in the program.

Parameters	Single	Linear	Circuit
Cycle Time (mins)	10	4-5	2
Vertiport Width (ft)	144	144-216	216
Vertiport Length (ft)	144	216	576
Safety Length (ft)	48	48	48

3.3.3.3 Throughput Equations

The following equations were the specific equations used in the code to find the number of flights per hour for a particular location. These calculations only work for a given area that is in the shape of a rectangle.

If the shorter side of the given area is longer than the longest side of the vertiport, the following equation is used to calculate the maximum number of vertiports a location can accommodate.

$$Number\ of\ Vertiports = \frac{Longer\ Side + Safety\ Area\ Side}{Shorter\ Side\ of\ Vertiport} \times \frac{Shorter\ Side + Safety\ Area\ Side}{Longer\ Side\ of\ Vertiport}$$

The Single and Linear topographies are limited to two rows of vertiports because vertiport pads require access to the side of the given area. This prevents air taxis from needing to fly over each other. The Circuit topography, however, ensures that the vertiport pads are already near the edge.

The final throughput is calculated using the following equation, with the cycle time and number of vertiports calculated previously.

$$Flights\ Per\ Hour = \frac{60}{Cycle\ Time} \times Number\ of\ Vertiports$$

3.3.4 Vertiport Location Diagrams

After we had gathered all necessary information about each location's throughput and optimal topography, we created models for each site. To create the layout for the different topographies, we made several assumptions. This included not accounting for the proximity to surrounding obstacles, not adding storage areas, not accounting for ground buffer zones, and not considering transportation from the vertiport site to the terminals.

Based on the FAA regulations[11], the safety areas that bordered the edge of the allocated area, if necessary, were removed to allow for more room for terminals and walkways. This adjustment was made with relevant FAA guidance to ensure safety levels were maintained.

As each site was mapped out, we considered many factors, including optimizing the space to allow for the greatest area for terminals and walkways, safe access to each gate/vertiport without people interfering with eVTOL operations, and adding the greatest possible number of vertiports we could within the dedicated area. To efficiently utilize the space, we combined several vertiport topographies within the same site.

This approach prioritized efficient eVTOL operations and spatial optimization while recognizing that real-world constraints, such as buffer zones, obstacles, and transport routes, were beyond the focus of the initial conceptual study.

3.4 Optimal Air Taxi Routing

To find optimal air taxi routes out of the airport, we utilized the heat map images from subsection 3.2 and the A* pathfinding algorithm. The A* algorithm uses a cost-based system to find the best path between the starting node and the ending node. The same destination points were chosen as the vertiport placement heat map, with the exception of San Francisco and Oakland, resulting in 9 destination points. Since the ending destinations were all outside of the air traffic heat map, we used the haversine formula to estimate the closest border cell to the target destination.

Given:

$$\theta = \frac{d}{r} \tag{10}$$

Where r is the radius of the sphere, d is the great circle distance between the two points, and θ is the angle between them,

$$\text{hav}\theta = \text{hav}(\Delta\varphi) + \cos(\varphi_1)\cos(\varphi_2)\text{hav}(\Delta\lambda) \tag{11}$$

Where,

- φ_1, φ_2 are the latitudes of point 1 and latitude of point 2,
- λ_1, λ_2 are the longitude of point 1 and longitude of point 2,
- $\Delta\varphi = \varphi_2 - \varphi_1$, $\Delta\lambda = \lambda_2 - \lambda_1$,

And,

$$\text{hav}\theta = \sin^2\left(\frac{\theta}{2}\right) \tag{12}$$

Then,

$$d = 2r \arcsin\left(\sqrt{\sin^2(\frac{\Delta\varphi}{2}) + \cos\,\varphi_1 \cdot \cos\,\varphi_2 \cdot \sin^2(\frac{\Delta\lambda}{2})}\right) \tag{13}$$

This final formula allows us to find the distance between any two points given their respective latitudes and longitudes. We use this to find the distance of a path when running the A* algorithm, and to find the closest border cell to our POIs. We made one alteration to this formula: Instead of arcsin, we used $\arctan^2$. This is because arcsin is unstable at numbers approaching 0 and 1 (which our model did, covering a mere 285 sq. mi.), producing floating point errors. $\arctan^2$, however, is much more stable.

The closest border cell was used as the ending node for the A* program. The A* algorithm calculates a least cost path by minimizing the function

$$f(n) = g(n) + h(n) \tag{14}$$

where $f(n)$ is the total cost of a path, n is the current node, $g(n)$ is the cost of the path from the start node to n, and $h(n)$ is a heuristic that estimates the cost of the cheapest path from n to the end node. Nodes, in our case, are cells. Also included in our cost calculation was a penalty score, calculated by multiplying a penalty weight (500) by the normal score of a cell, leading to our final cost function below:

$$f(n) = g(n) + h(n) + 500(S_{Normal}) \tag{15}$$

This ensured that the algorithm would avoid high-traffic cells whenever possible, but would still utilize a cell with traffic if necessary. This approach was repeated 5 times, once for only the first 6 hours of every day, once for the second 6 hours, once for the third 6 hours, once for the fourth 6 hours, and lastly, once for all 24 hours of every day. This produced 5 maps that showed optimal air taxi routes in differing traffic conditions.

4 Results

4.1 Air Traffic

Using data spanning 6 months from OpenSky, we plotted air traffic under 3,000ft on a map of 285 square miles surrounding SJC. The map was highlighted on a $\log_{10}$ scale based on the traffic density in a particular area. Using this method, we produced 4 heat maps that showed traffic around SJC for 6-hour increments across the day (Figure 17).

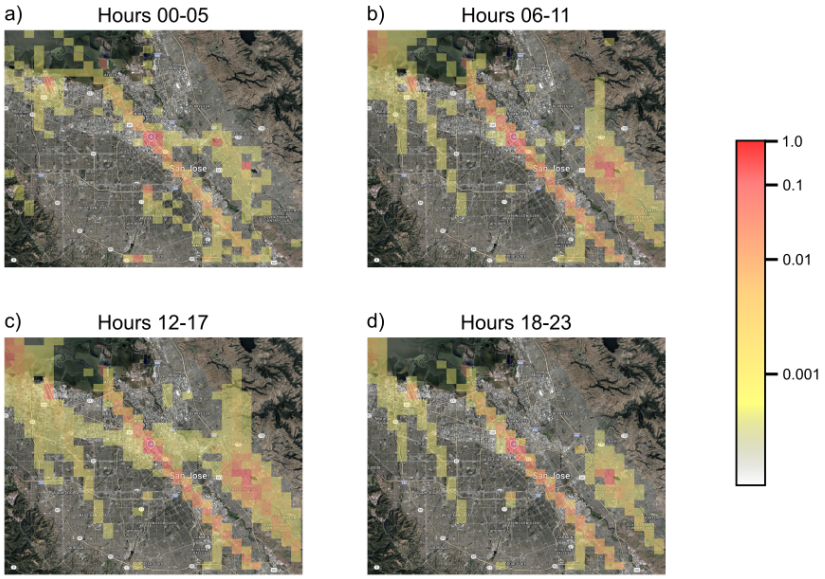

Figure 17: SJC Traffic Normal Scores Visualized on Log Scale (6-Hour Increments)
Imagery ©2025 Google, Vexcel Imaging US, Inc., Airbus. Imagery dates: 08 Aug. 2015–21 June 2025.

Additionally, we made heat maps for the entire day (24 hours) (Figure 18) and for the days that fell in the upper 5% of traffic (Figure 19).

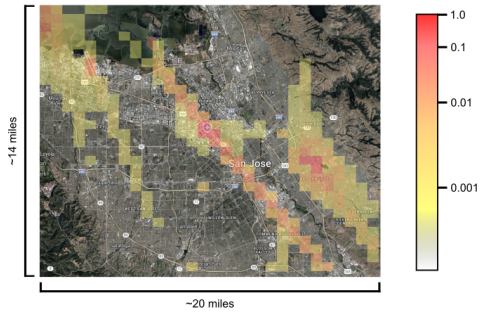

Figure 18: SJC Traffic Normal Scores Visualized on Log Scale (24 Hours)

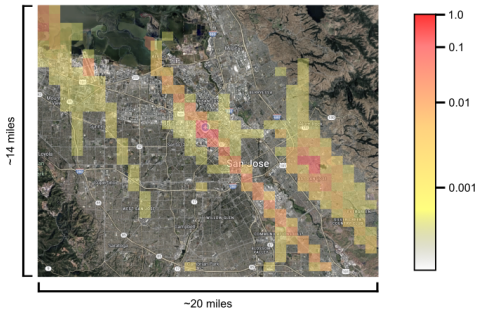

Figure 19: SJC Traffic Normal Scores Visualized on Log Scale (Top 5%)

Imagery ©2025 Google, Vexcel Imaging US, Inc., Airbus. Imagery dates: 08 Aug. 2015–21 June 2025.

In general, across all maps, the bulk of the traffic fell in 3 areas: the runway, the top-left corner (extending downwards), and the bottom-right corner (extending upwards). We interpreted both the bottom-right and top-left corner traffic as traffic from planes taking off from SJC. As these planes turn around, they briefly go above our 3,000ft limit, then come back under it, proceeding to the edge of the map.

The exception for these are the maps that covered hours 0000-0500 and 1200-1700 (Figure 17). The map for hours 0000-0500 had substantially less traffic than the other maps, with highlighted zones much smaller than the other maps. In contrast, the map for hours 1200-1700 had a fourth area of traffic concentration: a line of traffic, roughly horizontal, connecting the 3 other traffic concentrations. We interpreted this as being ambient traffic. The map of the 5% busiest days (Figure 19), as well as the map of the full 24 hours (Figure 18), both had hints of this fourth traffic concentration around the main area of the airport.

4.2 Possible Vertiport Locations

After running our location model, we obtained several maps modeling the feasible locations for a vertiport. The model can generate maps for thousands of different times depending on the decision of the operator. However, for this study, we will only show a select number of discrete timings that we have decided hold the most significance.

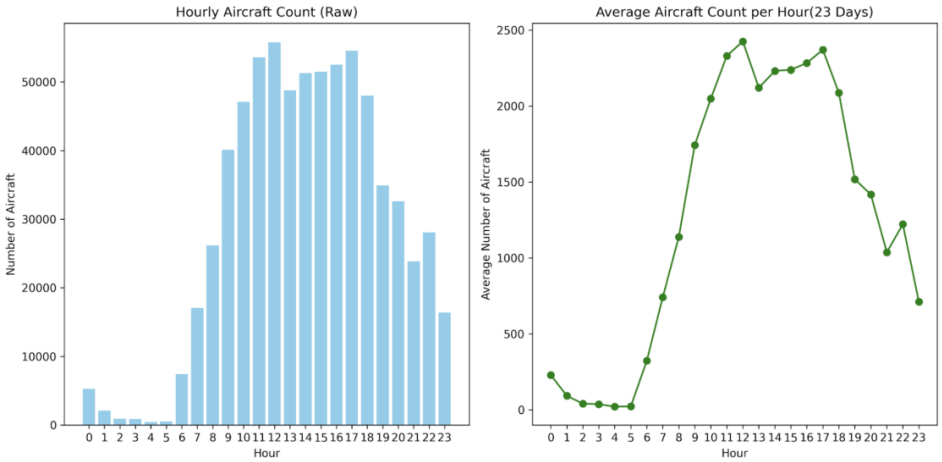

Figure 20: SJC Hourly Traffic by Raw Count (Left) and Average (Right)

As shown in Figure 20, the hours with the most air traffic are early afternoon (Hour 13) and evening

(Hour 18). Due to this, it would be appropriate to represent the possible locations using wind data at these two hours, as air taxis would most likely take off under wind conditions at these times.

From 1PM(Hour 13), we examined five heat maps, four of which correspond to discrete days across the 6 months analyzed. The dates selected were January 15, March 15, May 15, and June 15. This selection provided a wide array of seasonal wind conditions that can be present during air taxi operations throughout the year.

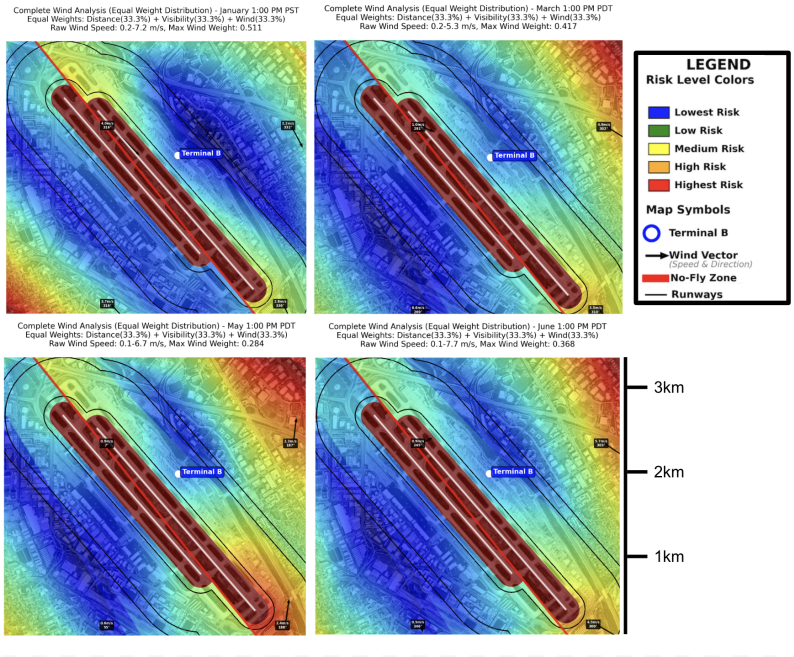

Figure 21: 4 Heat Maps at 1 PM
Imagery ©2024 Google, Vexcel Imaging US, Inc. Imagery dates: 11 Mar. 2022–18 July 2024.

As shown in Figure 21, there are clear shifts in the optimal (blue) area for where a vertiport can be placed. Regardless of these shifts, many areas remain consistently blue. The areas immediately toward the bottom left and the top right of the runway seem to be the most consistent locations to place a vertiport. However, further at the top right, there are large shifts in where we can place a vertiport, likely attributable to shifts in wind patterns over the year.

With this visualization of four distinct days at 1 PM across 6 months, there is bound to be a lot of variation between these intervals of time and potential inaccuracies of the data chosen. To combat this issue, we can refer to the heat map that shows the average wind favorability at 1 PM (Figure 22).

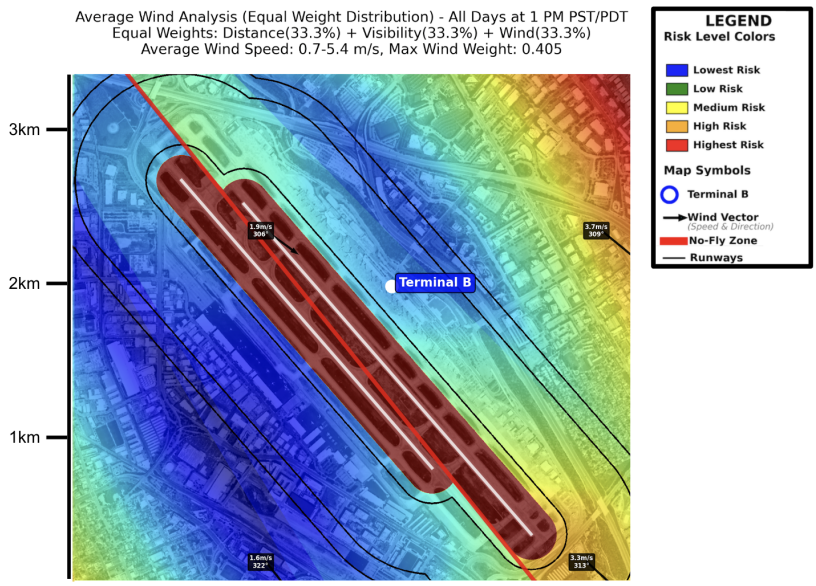

Figure 22: Averaged Heat Map at 1 PM
Imagery ©2024 Google, Vexcel Imaging US, Inc. Imagery dates: 11 Mar. 2022–18 July 2024.

This heat map is similar to the previous 4, with two blue regions to the immediate top right and bottom left of the runway. This demonstrates that the discrete hourly intervals shown earlier are representative of a large portion of the 6 months of possible wind patterns.

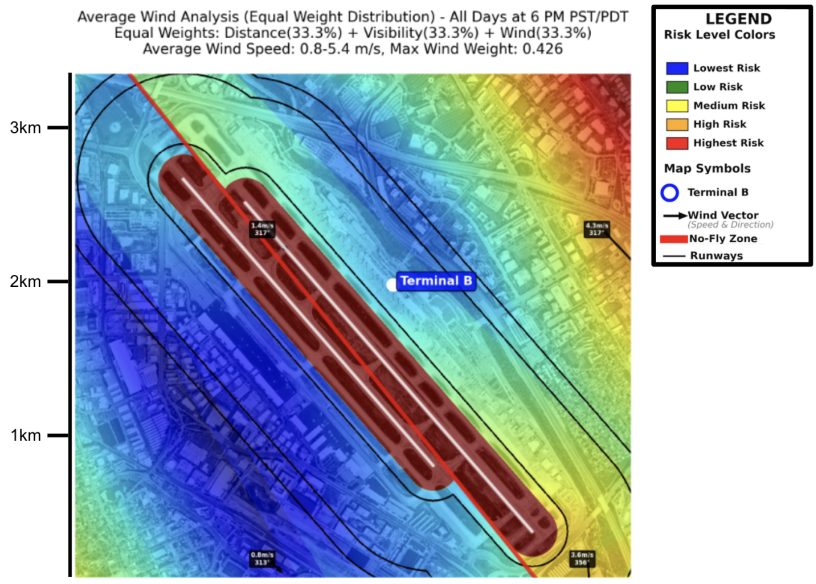

Figure 23: Averaged Heat Map at 6 PM
Imagery ©2024 Google, Vexcel Imaging US, Inc. Imagery dates: 11 Mar. 2022–18 July 2024.

Figure 23 is an average of wind patterns for all days at 6 PM PST/PDT. The map is very similar to the 1 PM 6-month average. However, upon closer inspection, the wind arrows are slightly different

in terms of direction and magnitude, showing signs of variability. Overall, the averages at both times are visually similar, showing that wind patterns at SJC may not experience much variability, which shows the accuracy of the discrete time intervals.

4.3 Vertiport Configuration Diagrams

The following diagrams show the optimal topographies for every location (Figure 2). We tried multiple topographies, and these gave the highest throughput.

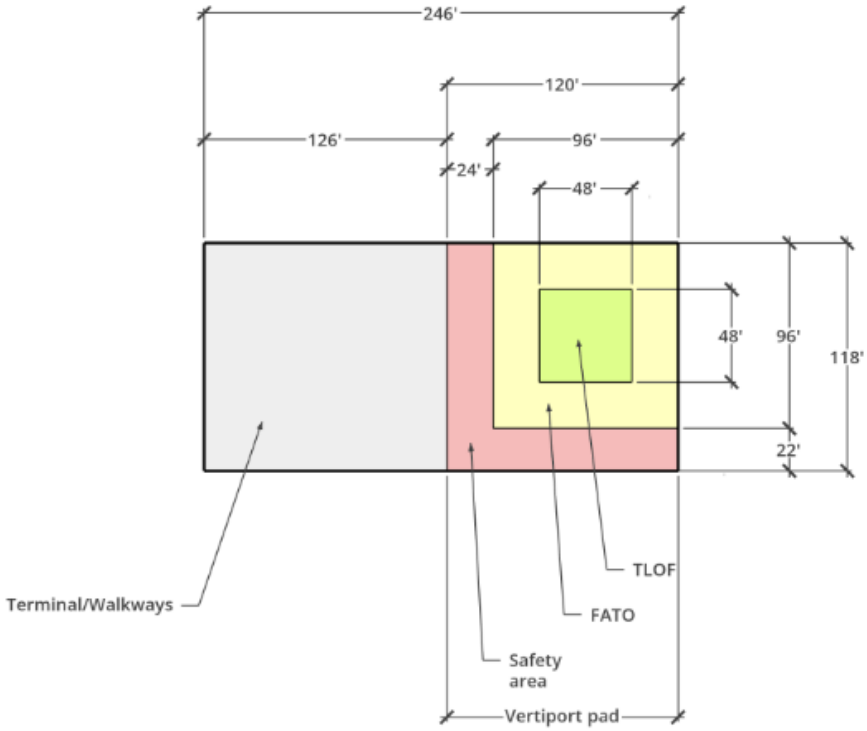

Figure 24: Location 1 (6 flights/hr — Space For Terminal: True)

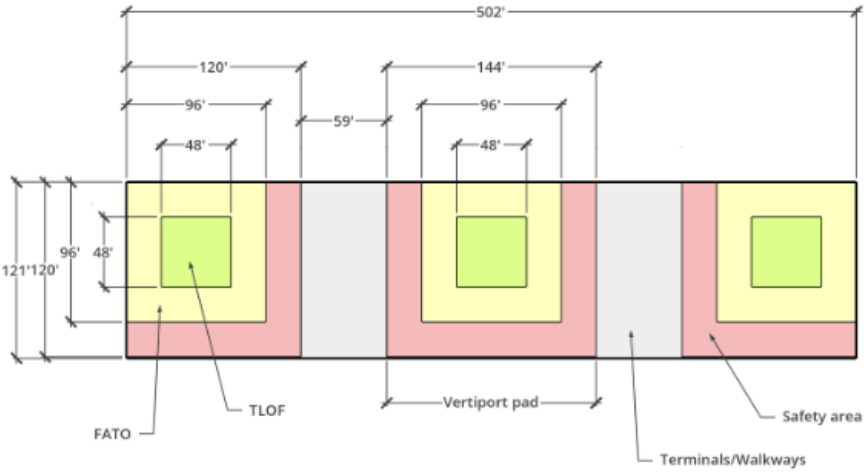

Figure 25: Locations 2 and 3 (18 flights/hr — Space For Terminal: False)

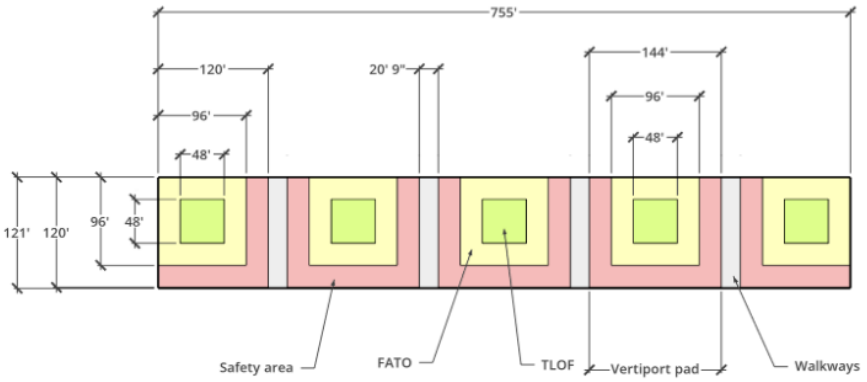

Figure 26: Location 4 (30 flights/hr — Space for Terminal: False)

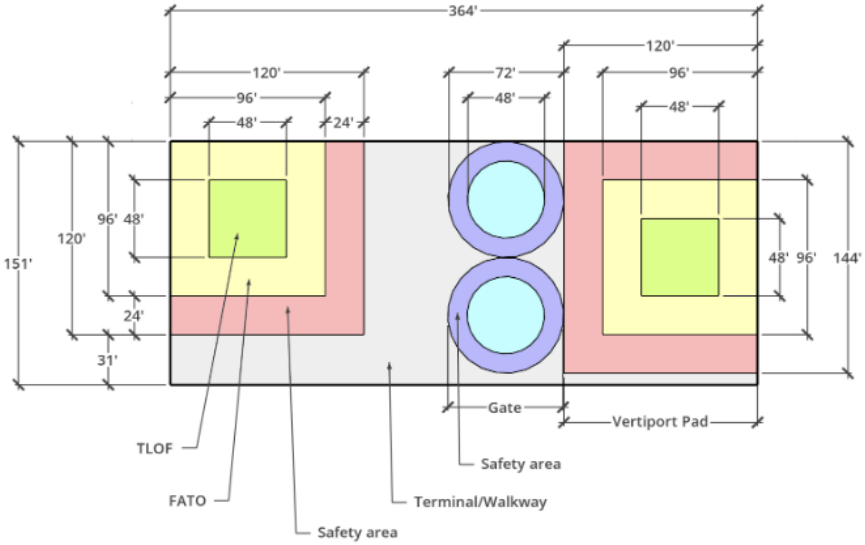

Figure 27: Location 5 (18 flights/hr — Space For Terminal: False)

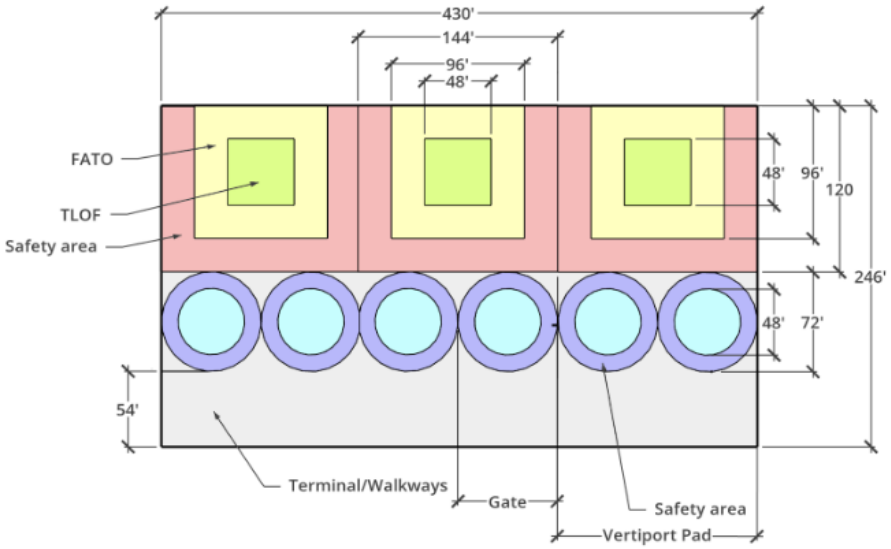

Figure 28: Location 6 (36 flights/hr — Space For Terminal: True)

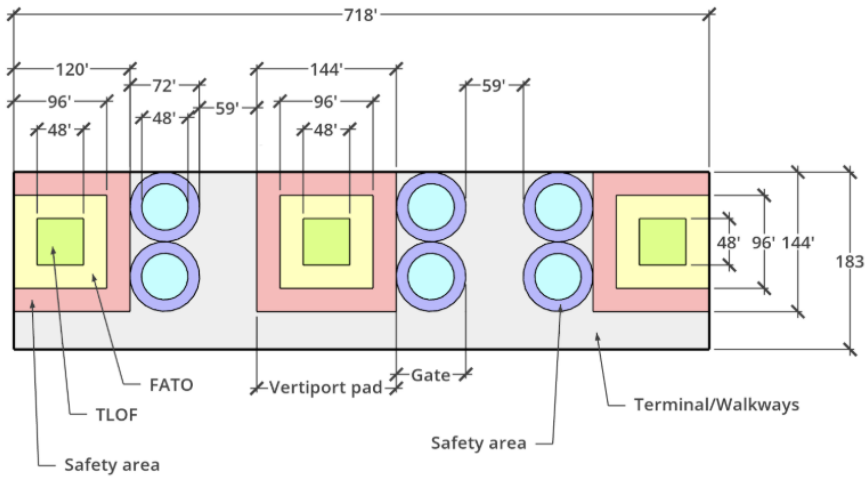

Figure 29: Location 7 (36 flights/hr — Space For Terminal: False)

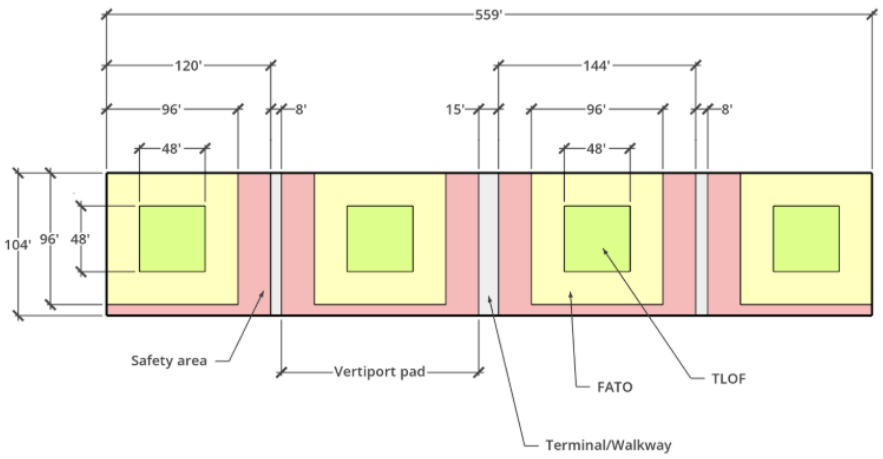

Figure 30: Location 8 (24 flights/hr — Space For Terminal: False)

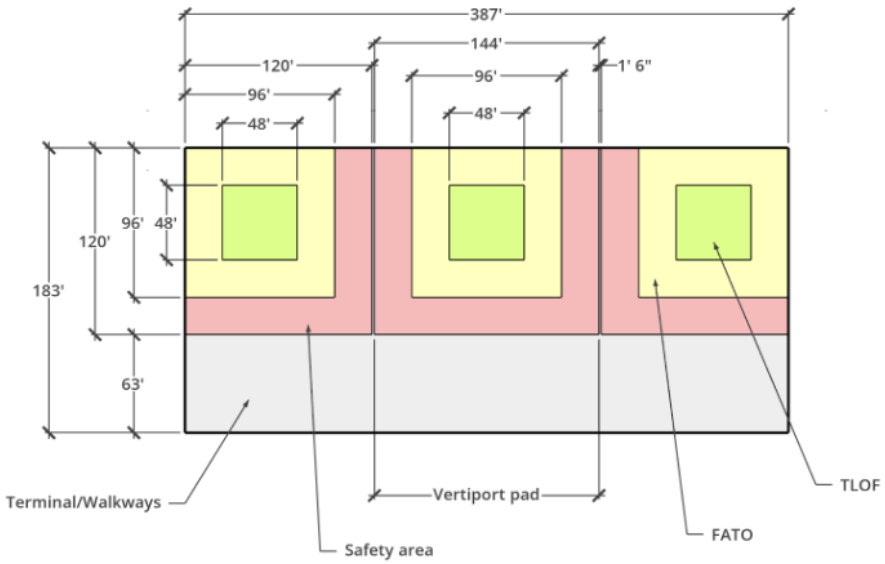

Figure 31: Location 9 (18 flights/hr — Space For Terminal: True)

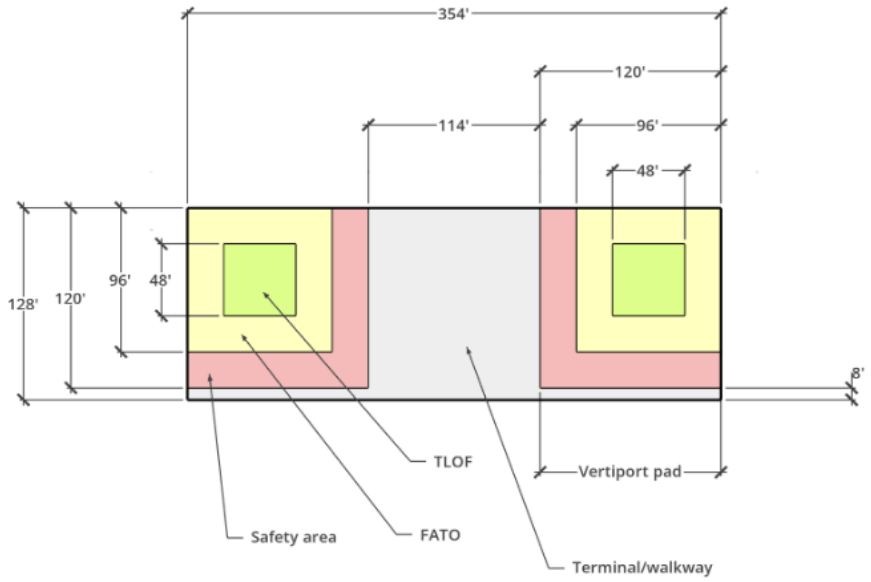

Figure 32: Locations 10 and 11 (12 flights/hr — Space For Terminal: True)

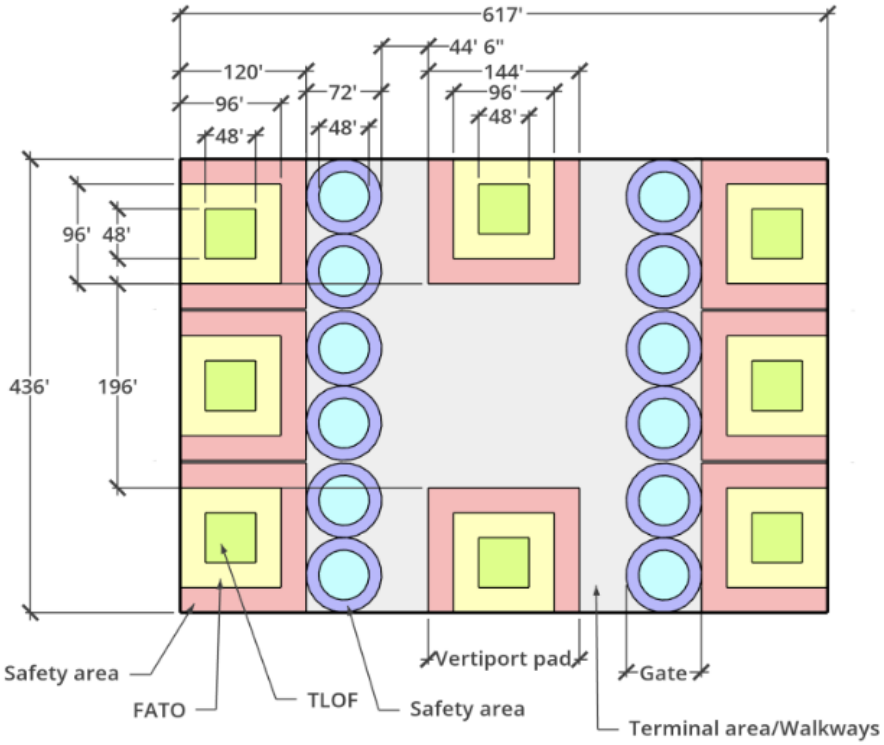

Figure 33: Location 12 (84 flights/hr — Space For Terminal: True)

We later narrowed these twelve locations down to three final locations.

4.4 Optimal Air Taxi Routing

We used the A* algorithm to find optimal paths from three different vertiport locations to POIs. The algorithm was penalized for distance and for traveling through high traffic density, and chose

paths with the lowest score. This process produced 6 maps for each location with several paths to different POIs on it: one for all 24 hours, one for each 6-hour increment, and one for the 5% busiest. These paths were layered on the air traffic density heat map for easy visualization. Each POI was given a different colored route.

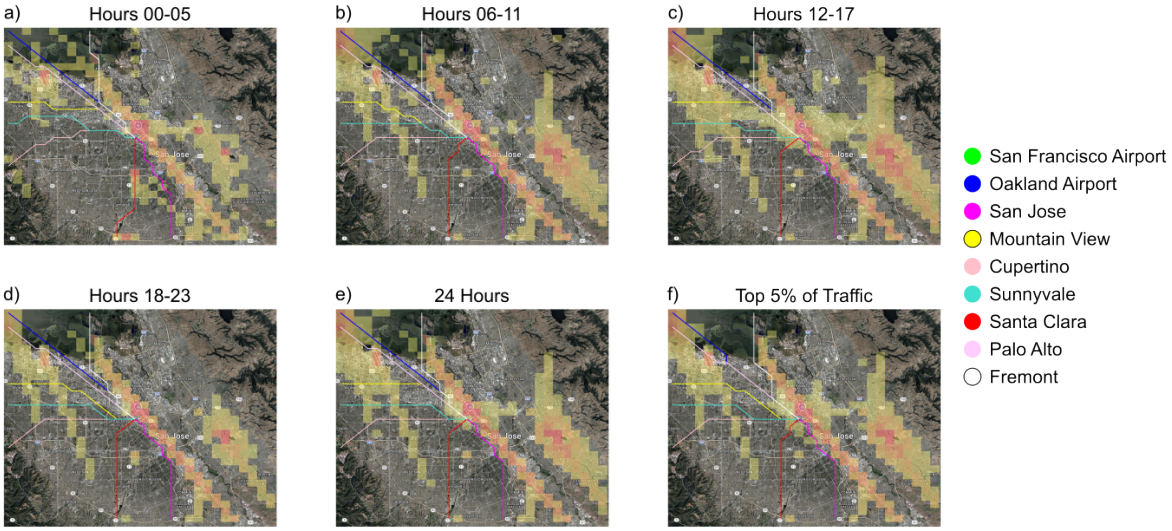

Figure 34: A* Routes for Location 6
Imagery ©2025 Google, Vexcel Imaging US, Inc., Airbus. Imagery dates: 08 Aug. 2015–21 June 2025.

The first location tested was location 6, which was situated roughly Southwest of the runways (Figure 34). Certain routes did not change throughout the different maps, such as the route to Oakland Airport, while some changed frequently, such as the route to Fremont. One additional thing we noticed was that the starting tile for location 6 was not colored for 4 out of 6 maps, and colored yellow for the other two. Furthermore, for hours 0000-0500, 0600-1100, and 1800-2300, 4 out of 8 surrounding tiles were uncolored. For hours 1200-1700, 3 of those 4 tiles were colored yellow, with the 4th being uncolored.

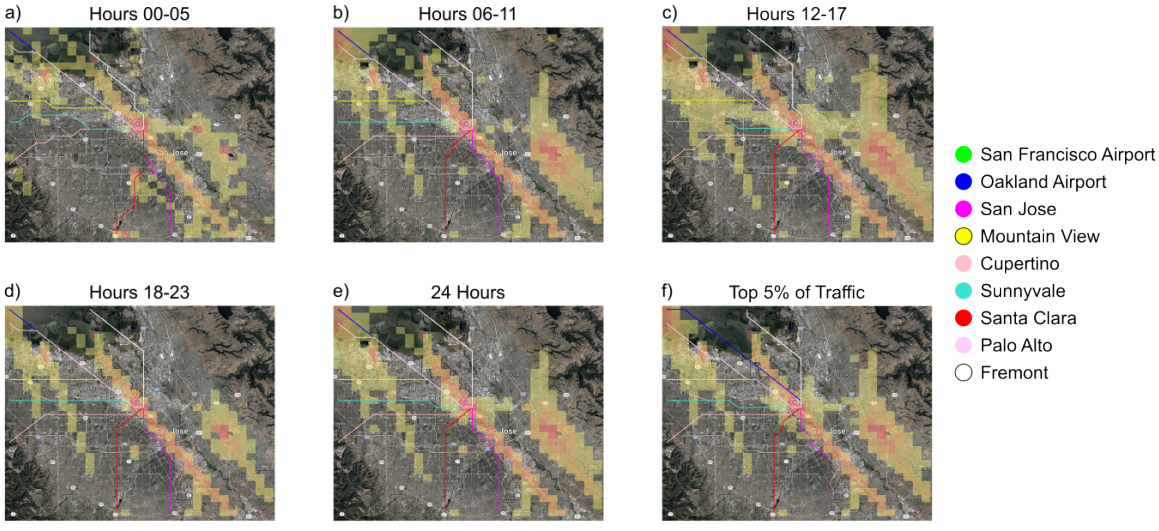

Figure 35: A* Routes for Location 7
Imagery ©2025 Google, Vexcel Imaging US, Inc., Airbus. Imagery dates: 08 Aug. 2015–21 June 2025.

The second location tested was location 7, which was situated to the east of the runways (Figure 35).

This location lies in a very high-traffic area, as evidenced by the fact that the starting tile for routes coming from this location was always colored red. Some routes, to get to their destination, had to travel through the red tile with the most traffic (normal score of 1.0). Since most of the routes had destinations in the West, almost all routes had to cross the large line of traffic-dense cells to reach their destinations. The surrounding tiles for location 7 were also almost always colored, with 2-3 of those surrounding tiles consistently being red. As such, routes from this location not only started in a high traffic cell, but also needed to traverse through other high traffic cells to their endpoint.

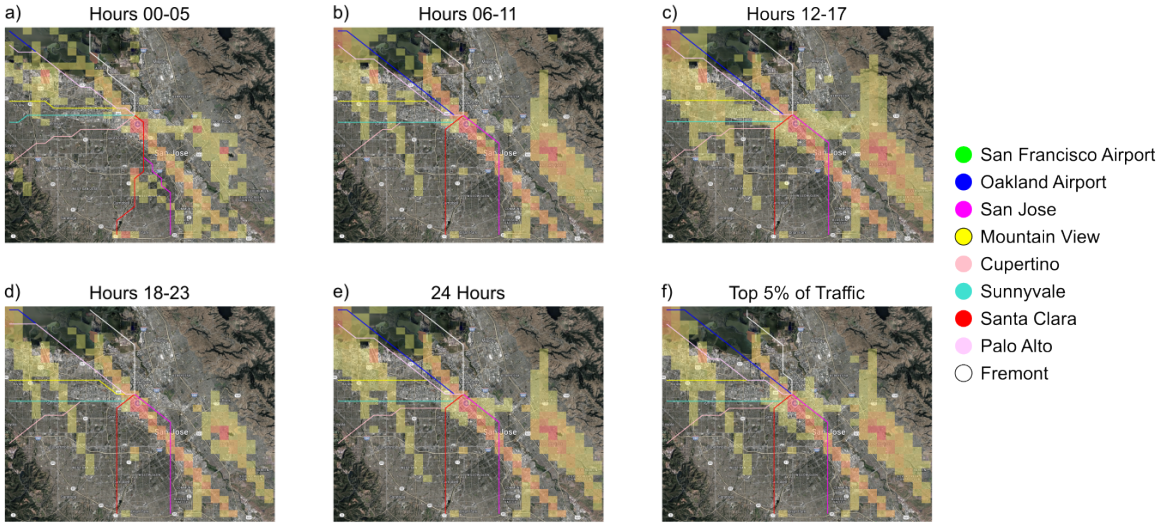

Figure 36: A* Routes for Location 12
Imagery ©2025 Google, Vexcel Imaging US, Inc., Airbus. Imagery dates: 08 Aug. 2015–21 June 2025.

The last location tested was location 12, which is situated north of the runways. This location lies in a medium traffic area, as its starting cell was usually colored orange, with only one occurrence of it being colored red, in hours 0600-1100. Additionally, other than hours 1200-1700, the surrounding tiles for this location were generally low traffic. Two surrounding cells were consistently colored orange, one consistently colored red, and the others were generally yellow or uncolored. Routes from this location generally never passed through the red cell. The exceptions to this are the routes to San Jose and Santa Clara during the hours 0000-0500, where they passed through two red tiles and an orange tile. Routes from this location that passed through the orange cells generally subsequently passed through uncolored cells. Only one route consistently showed trouble: the route to San Jose. This route, for all maps except for hours 0000-0500, had to pass through several orange and red cells to reach its destination, needing to cut through the Southern tail of the runway traffic concentration.

5 Discussion

5.1 Air Traffic

For this study, our goal was to integrate air taxis into SJC with minimal interruptions to the airport's normal operations. As such, we aimed to use the air traffic heat map to find out how we could incorporate air taxi traffic without crossing into existing airplane traffic under 3,000 ft. The air traffic heat maps allow us to see where airplane traffic occurred over the first 6 months of 2022, so that it may be avoided. For a more up-to-date analysis, new CSV files may simply be provided to existing code. As mentioned in the results section, airplane traffic is mostly present in three areas of concentration: the runway, the top left corner, and the bottom right corner. These highlights present areas that should ideally be avoided by air taxis. However, due to the log scale coloring, cells highlighted in yellow have 10x less traffic than cells highlighted in orange, and 100x less traffic than cells highlighted red. Therefore, we deemed that infractions into yellow cells are acceptable, orange cells tolerable, and red cells highly discouraged. Principally, what caught our interest in these heat

maps was the runway traffic concentration. Across all maps, this traffic concentration stretched from the bottom edge of the map to the top edge of the map. This presented a consideration for when we placed our vertiports in the airport. We wanted to avoid crossing this center line as much as possible to minimize disruptions to existing traffic. The map of hours 1200-1700 presented an extra consideration for us, the fourth traffic concentration. We also utilized the difference in traffic between hours 0000-0500 and hours 1200-1700. As these timeslots had the least and most traffic, respectively, we used them as our best and worst case scenarios later in the project.

5.2 Possible Vertiport Locations

Before diving into the significance of the heat maps, it is important to highlight some of their shortcomings. For the first four maps, discrete times were used to simulate the variability in the wind at SJC. However, a drawback to this method is that other wind variations may be neglected by only focusing on a small set of times. Despite this, we felt that analyzing wind data at only specific intervals of time (hours of highest traffic) would be sufficient for this study, as analyzing every hour separately could prove too complex.

We still decided to represent all the hours at 1 PM and 6 PM (PST/PDT) through an average of all wind vectors in the bounds of SJC. By averaging all wind vectors over the 6 months at set times, we were able to account for much of the variation not described in the other images when generating a heat map. Additionally, many of the visual patterns of the averaged 1 PM map were common across the discrete hourly maps, signifying that the averaged maps were an accurate representation of each day.

Looking at any of the images, it is easy to notice two large blue regions on either side of the runways. The regions in Figure 22 are outlined in Figure 37. These zones are the most optimal as they are closest to runways; terminal B, in optimal wind conditions, has access to several important destinations, and stay out of no-fly zones. On every heat map, the blue zone on the bottom left is larger than the other blue zone, regardless of time or wind condition. This may be attributed to a variety of factors. Even though the blue area on the bottom-left is further from the terminal itself, it is situated at an optimal location where it has access to several important destinations. This may have boosted cell scores, giving the area a blue color.

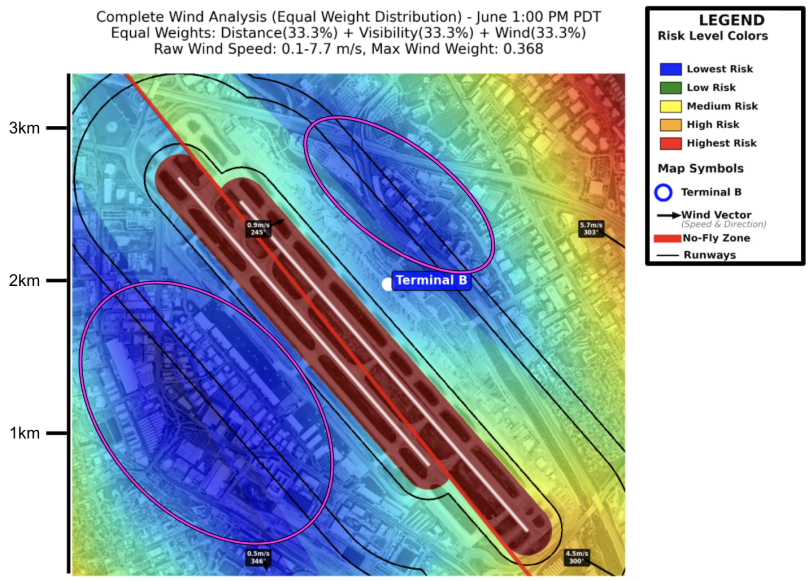

Figure 37: Averaged Heat Map at 1 PM
Imagery ©2024 Google, Vexcel Imaging US, Inc. Imagery dates: 11 Mar. 2022–18 July 2024.

However, despite the bottom-left having a better score than the top-right region, it is important to

consider the logistical factors. Mainly, the proximity of the bottom-left region to Terminal B makes any vertiport in that location far from passenger traffic, reducing efficiency and causing additional stress for airport infrastructure, as additional transportation is needed from the terminal to the vertiport. Even though the model accounted for this difference, it should be important to consider because several other factors, such as favorable access to POIs and runway distance, may outweigh the distance to Terminal B, as all variables were weighted equally. So, when constructing a physical vertiport, it is important to note these constraints for even the most optimal locations.

Despite this, the large region would prove to be a great vertiport hub due to its easy access to many important destinations, such as Santa Clara, San Francisco, and Palo Alto. On the other hand, the top-right area has access to Oakland and Fremont. Also, compared to the bottom-left region, the majority of the top-right region is outside the FAA's restricted zones defined in previous sections.

From looking at the benefits and drawbacks of both regions, it is reasonable to conclude that they are both beneficial for the operation of eVTOLs in SJC. They both cater to certain passenger traffic demographics and function independently in the presence of adverse wind and weather conditions. As a result, we concluded that it would be ideal to place a vertiport in each respective section, as that would increase the number of major destinations and allow a greater flow of eVTOL traffic through SJC.

5.3 Topography Analysis

5.3.1 Single

The Single topography was the only topography that could fit into many of the chosen locations, due to their narrow shapes. A Linear with a gate2pad ratio of 2 (Linear 2) could sometimes also be used, but that would either leave limited space for walkways/terminals, or there would be no change to the total throughput.

5.3.2 Linear

Even though Linear, with a gate2pad ratio of 3 (Linear 3), has the minimum cycle time for the Linear topography, we found that it was not efficient enough to make up for the extra area this topography uses. Linear 3's longer width also limits its use in narrower areas, unlike Linear 2, which has one side that is the same length as Single.

5.3.3 Circuit

Even though the Circuit topography has the shortest cycle time, the area the Circuit design takes up can fit three Linear 2 vertiports, which allows for 6 more flights per hour. The Circuit design does not use space efficiently enough to be practical. This topography was not used for any of the location diagrams. Another downside is that passengers would need to cross the taxiways to reach the gates. A potential mitigation to this problem would be to install stairs between the gates that lead to a lower level.

5.3.4 Optimal Topography

Linear 2 was found to be the most optimal topography as it has the highest throughput for the smallest area used. For many of the larger locations, Linear 2, combined with some Single vertiports, allowed for even higher throughputs. For further experiments, variations of the Linear and Circuit design can be tested to find the most systematic design. If the time spent in the gate increases or the charging time is accounted for, a higher gate2pad ratio could potentially be beneficial.

5.4 Viable Vertiport Locations

When deciding the final locations, several factors were carefully considered as we aimed to optimize the efficiency of the eVTOL operations. The main consideration was the site throughput, which led to the exclusion of most of the sites with insufficient capacity - location 1, 2, 3, 4, 5, 8, 9, 10, and 11. Based on previous research done on the Cologne Airport, Bonn - a facility of similar size with similar public transport access to SJC[4] - we calculated that around 540 flights would take place every day.

Based on our hourly aircraft count map (Figure 20), we assumed that the air taxis would be running for 17 hours a day during peak hours from 6:00 to 23:00. Next, we evaluated the geographical location and terminal/walkway areas of each site.

Regarding location, we wanted to add one vertiport site on each side of SJC - one on the West and one on the East - as there are key destinations found on either side of the airport. This would minimize eVTOLs' flight paths needing to cross the runways, which have high volumes of air traffic, reducing the risk of collisions and enhancing operational safety.

In terms of terminal and walkway areas, we selected the topographies with the largest areas for terminal and walkway construction to ensure safety and customer comfort.

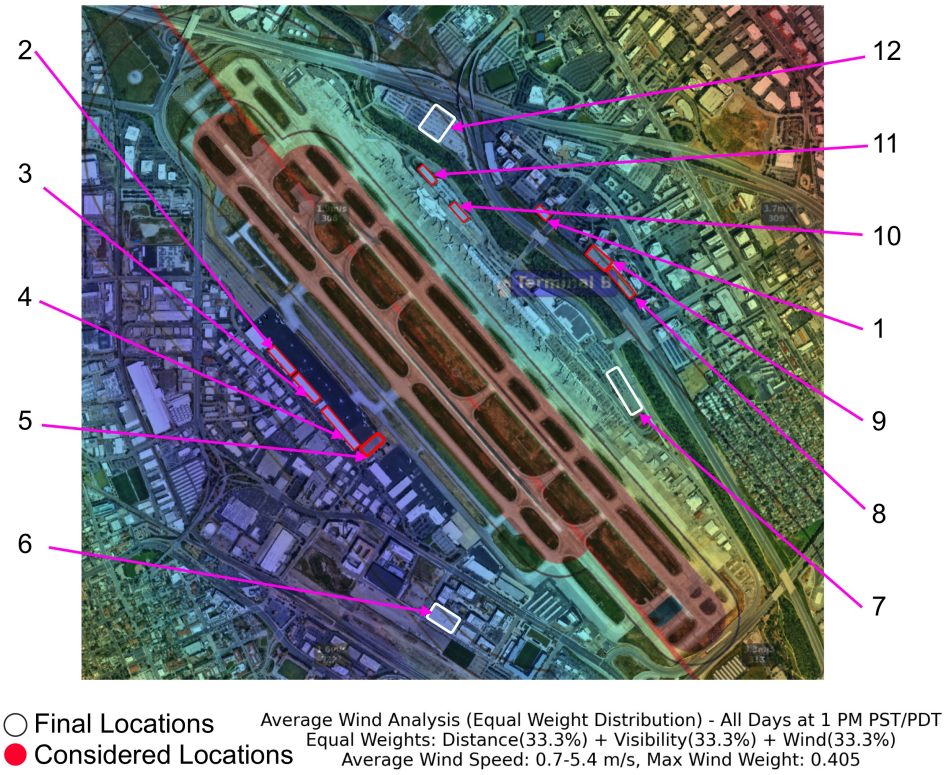

Figure 38: Three Viable Locations
Imagery ©2024 Google, Vexcel Imaging US, Inc. Imagery dates: 11 Mar. 2022–18 July 2024.

5.4.1 Location 6

Location 6 (Figure 28) has over 612 flights per day, therefore exceeding the initial air taxi demand, and is located on the west side of the airport. Furthermore, it has adequate space for terminals and walkways and is near a major roadway, which allows for quick access to the terminal. A drawback of this location is that it utilizes a stadium parking lot, which means that it may not be feasible.

5.4.2 Location 7

Location 7 (Figure 29) has over 612 flights per day, therefore exceeding the initial air taxi demand, and is located on the east side of the airport. Furthermore, it has adequate space for walkways and is located near the terminals, making the travel time between the vertiports and terminals minimal. However, it does not have enough room for terminals, meaning that people would not be able to sit and wait for their air taxi in a sheltered area.

5.4.3 Location 12

Location 12 (Figure 33) has over 1428 flights per day, which makes it the location with the highest throughput, greatly exceeding the initial demand for air taxis. It is located on the east side of the airport and has enough room for terminals and walkways. Furthermore, there is already an established bus shuttle service from this parking lot (economy lot 1) to the terminals, making the issue of travel between the vertiport and airport already resolved.

5.5 Air Taxi Route Planning

While we produced 6 maps per location, for the Discussion part of this project, we will be looking at only hours 0000-0500 and hours 1200-1700. We chose these time intervals as they are the times with the least and most traffic, respectively.

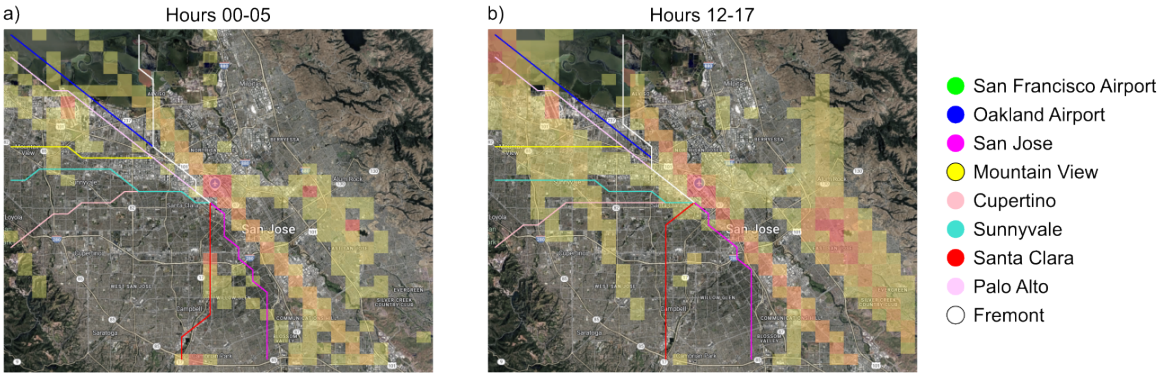

Figure 39: TA* Routes for Location 6 (Hours 0000-0500 and 1200-1700)
Imagery ©2025 Google, Vexcel Imaging US, Inc., Airbus. Imagery dates: 08 Aug. 2015–21 June 2025.

Location 6 (Figure 39) performed rather consistently in low and high periods of traffic. Routes remained relatively consistent, and seldom passed through a cell highlighted by anything other than yellow. The exception to this is the upper left corner of the map, where, during periods of high traffic, the target cells for the routes to Oakland Airport, San Francisco Airport, and Palo Alto are colored red. However, as this is an unavoidable problem regardless of vertiport location, we disregard it when evaluating vertiport effectiveness. Routes in location 6 also minimally had to cross traffic concentrations. During low traffic hours, only one route crosses a traffic concentration: the route to Fremont crosses the north tail of the runway traffic concentration. In periods of high traffic, routes cross through the traffic concentration stemming from the top left corner, passing through all yellow cells.

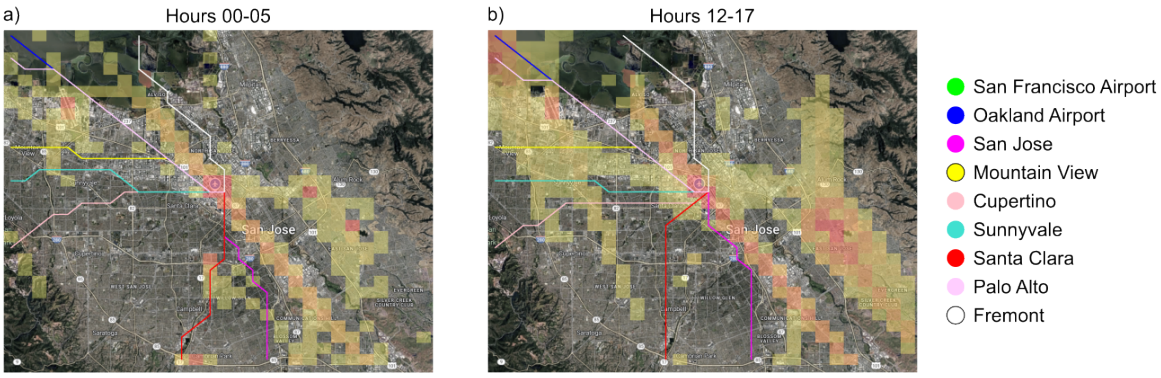

Figure 40: A* Routes for Location 7 (Hours 0000-0500 and 1200-1700)
Imagery ©2025 Google, Vexcel Imaging US, Inc., Airbus. Imagery dates: 08 Aug. 2015–21 June 2025.

Location 7 (Figure 40) performed consistently poorly to our standards. In both periods of low and high traffic, the start cell for this location was always colored red. In both low and high traffic, routes had to cross the runway traffic concentration to get to their destination. This is likely because, from our selection of POIs, we anticipated most air taxi traffic from SJC heading west. Placing this vertiport on the east side of the runway necessitates crossing through very busy airspace to get to target locations. As such, the issue with location 7 is less that it performs worse under high traffic conditions, and more that it performs poorly regardless of the relative density of traffic.

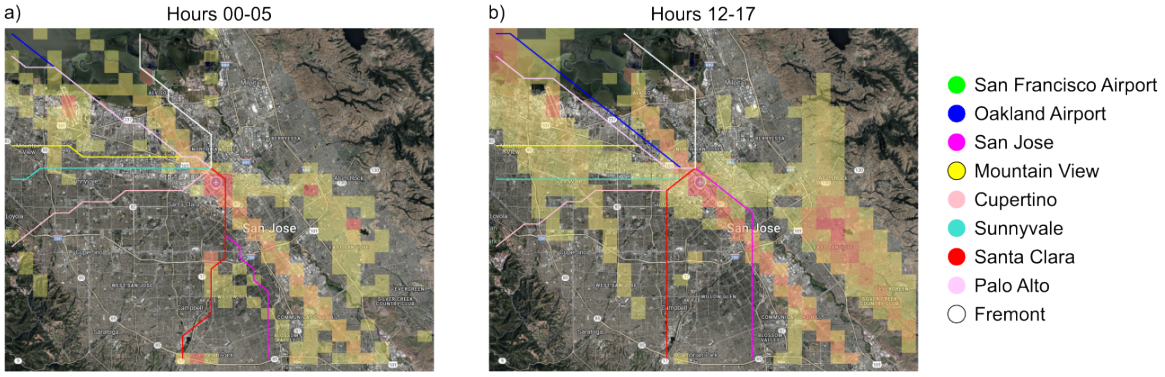

Figure 41: A* Routes for Location 12 (Hours 0000-0500 and 1200-1700)
Imagery ©2025 Google, Vexcel Imaging US, Inc., Airbus. Imagery dates: 08 Aug. 2015–21 June 2025.

Location 12 (Figure 41) performed well under low traffic conditions, but faltered under high traffic conditions. In low traffic conditions, the airspace above the vertiport was colored yellow-orange, indicating a low to medium amount of traffic. Routes coming from this location during low traffic hours had to cross the north tail of the runway traffic concentration, but the cells they passed through were generally colored yellow, and after passing through the traffic concentration, the routes generally proceeded through uncolored or, rarely, yellow-colored cells. Under high traffic conditions, however, routes from this vertiport consistently pass through high traffic areas. Under high traffic conditions, the airspace above the vertiport became colored orange-red, indicating a high amount of traffic. Additionally, the north tail of the runway traffic concentration became busier during hours 1200-1700, leading to more red and orange-colored cells. As a result of the vertiport's placement north of the runways, routes coming from this location had to pass through these busier cells to reach their destinations.

Overall, when evaluating the three locations, we looked at the traffic conditions surrounding the location, how the routes interacted or interfered with airplane traffic, and how the routes responded to differing traffic conditions. In our analysis, location 6 performed best overall, with location 12 as the runner-up, and location 7 as the worst.

5.6 Final Vertiport Locations

Based on the route planning and throughput analysis, we chose location 6 as our final vertiport location. Location 6's throughput exceeds the daily number of flights needed, and route planning shows little to no interference with high airplane traffic areas.

If eVTOL operations were to expand, Location 12 is the backup location due to its large throughput and existing methods to easily go from this location to the airport terminals. Location 12 is an extra vertiport location because most of the key locations tested in route planning were on the west side. This means that most of the air taxis coming from the surrounding areas have to cross the airport to reach this vertiport, which would interfere with the high levels of air traffic already present. We deemed Location 7 an unsuitable place for a vertiport because it already has too much air traffic over its airspace.

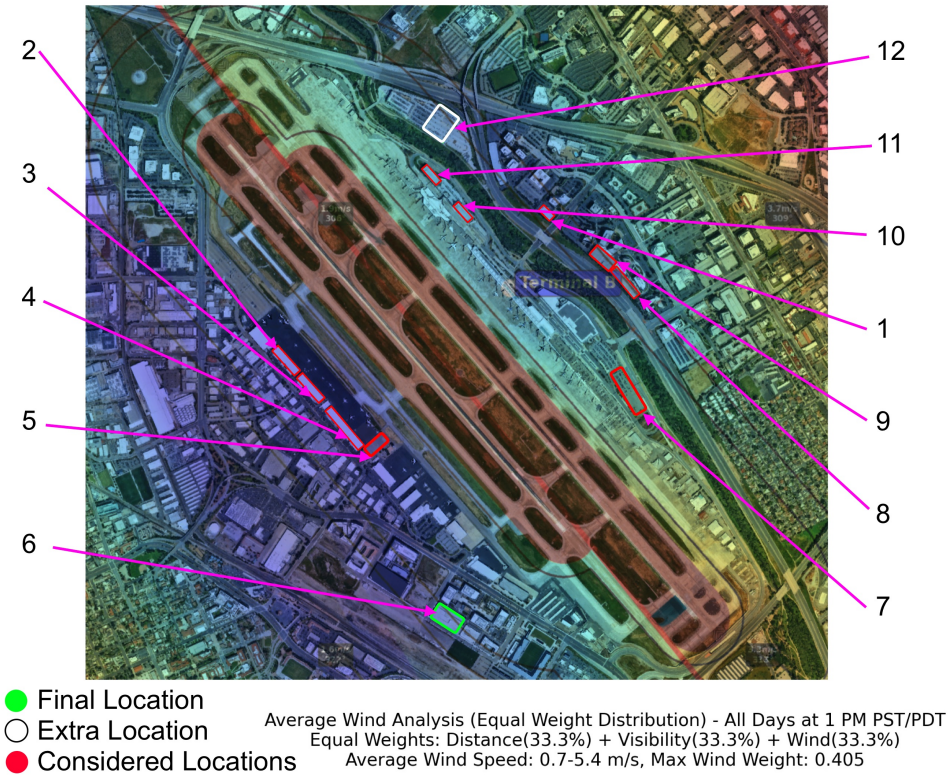

Figure 42: Final Vertiport Locations
Imagery ©2024 Google, Vexcel Imaging US, Inc. Imagery dates: 11 Mar. 2022–18 July 2024.

6 Conclusion

The integration of eVTOLs into major transport sites such as the San Jose Mineta International Airport (SJC) represents a crucial move towards reinventing urban transport. As congestion continues to increase, pressure on companies to integrate air taxis into an urban setting intensifies. However, integrating air taxis into airports creates a significant challenge as many factors need to be considered –including air traffic, noise, weather, proximity to the airport infrastructure, and eVTOL flight paths to key destinations from the airport.

This paper explores methods for efficiently integrating air taxis into SJC using spatial analysis, heat mapping, and route optimization algorithms. Using the heat maps, potential locations were found, which then underwent detailed analysis to estimate throughput and possible topographies. Finally, the A* pathfinder algorithm was applied to model flight paths for eVTOLs to nine key destinations around the airport, leading to the conclusion that location 6 was the optimal site, with location 12 serving as the backup location.

Location 6 supports a throughput of 612 flights per day, has adequate room for terminals and walkways, and is next to a major roadway, meaning that it has quick and easy access to the terminals. As location 6 was inputted to model out different flight paths, the paths rarely crossed high traffic density areas, except for the area in the upper-left corner of the map. However, since this area was crossed by all flight paths regardless of the vertiport location, its impact was deemed unimportant in the site selection process. Location 6 is located on the west side of the airport and would be built on an existing stadium parking garage. Airports can accommodate several vertiport locations, so if eVTOL demand increases, location 12 would be implemented, as it has a throughput of over 1428 flights per day.

While San Jose Airport features two parallel runways, the framework and methods developed in this study can be modified to fit any airport configuration. This study highlights the benefits of scalable, data-driven frameworks for eVTOL integration. As air taxis become more common, with Archer air

taxis servicing the 2028 L.A. Olympics, reliable and versatile methods for integrating eVTOLs will become increasingly important. By applying similar methods as used in this paper to airports around the country, incorporating air taxis into our infrastructure will become steadily more viable, paving the way for the next generation of sustainable transportation.

References

[1] J. Cannon, "Americans waste a week annually in traffic congestion, report says," Commercial Carrier Journal, Jan. 09, 2025. https://www.ccjdigital.com/business/article/15711348/americans-waste-a-week-annually-in-traffic-congestion-report-says

[2] Environmental Protection Agency, "Fast Facts on Transportation Greenhouse Gas Emissions," United States Environmental Protection Agency, Jun. 18, 2024. https://www.epa.gov/greenvehicles/fast-facts-transportation-greenhouse-gas-emissions

[3] MarketsandMarkets, "Urban Air Mobility Market Size, Share, Industry Report, Revenue Trends and Growth Drivers," MarketsandMarkets, 2025. https://www.marketsandmarkets.com/Market-Reports/urban-air-mobility-market-251142860.html?gad

[4] "VFS - Press Release: VFS Electric VTOL Directory Hits 1,000 Designs," Vtol.org, 2019. https://vtol.org/news/press-release-vfs-electric-vtol-directory-hits-1-000-designs

[5] N. Hagag and B. Hoeveler, "The feasibility of electric air taxis: balancing time-savings and co2 emissions - a joint case study of respective plans in Paris," CEAS Aeronautical Journal, Mar. 2025, doi: https://doi.org/10.1007/s13272-025-00811-8.

[6] INRIX, "Scorecard," Inrix. https://inrix.com/scorecard/#form-download-the-full-report

[7] B. L. Beckman, "Archer reveals eVTOL Maker that'll cost as much as Uber Black to fly," Mashable, Jun. 11, 2021. https://mashable.com/article/archer-maker-evtol-reveal

[8] "OST/R — BTS — Title from h2," Bts.gov, 2021. https://www.transtats.bts.gov/OT/Delay/OT/DelayCause1.asp?20=E

[9] "Slot Administration - U.S. Level 3 Airports — Federal Aviation Administration," Faa.gov, 2023. https://www.faa.gov/about/office_org/headquarters_offices/ato/service_units/systemops/perf_analysis/slot_administration/slot_administration_schedule_facilitation/level-3-airports

[10] "Evtol industry in the US (analysis) – Flying Cars Market," Flyingcarsmarket.com, Mar. 02, 2025. https://flyingcarsmarket.com/evtol-industry-in-the-us-analysis/ (accessed Aug. 08, 2025).

[11] luism@minima.es, "What are vertiports and how do they work? — Openvia," Openvia, Nov. 28, 2023. https://www.openvia.io/what-are-vertiports-and-how-do-they-work (accessed Aug. 08, 2025).

[12] M. Meyers, "Engineering Brief No. 105A, Vertiport Design, Supplemental Guidance to Advisory Circular 150/5390-2D, Heliport Design," Dec. 27, 2024. https://www.faa.gov/airports/engineering/engineering_briefs/eb_105a_vertiports (accessed Aug. 08, 2025).

[13] J. Weiner, "Charging Infrastructure is Slowing eVTOL Progress. Here's How We Can Move Forward.," SepiSolar, Aug. 2023. https://www.sepisolar.com/sepisolar-blogs/charging-infrastructure-is-slowing-evtol-progress-heres-how-we-can-move-forward/

[14] ICAO, "Annex 17," Icao.int, 2019. https://www.icao.int/Security/SFP/Pages/Annex17.aspx

[15] Sustainability Directory, "Urban Air Mobility Integration Challenges → Scenario," Prism → Sustainability Directory, Mar. 08, 2025. https://prism.sustainability-directory.com/scenario/urban-air-mobility-integration-challenges (accessed Aug. 08, 2025).

[16] P. Brinkmann, "Flying air taxis directly in and out of international airports could be problematic," Aerospace America, Sep. 09, 2022. https://aerospaceamerica.aiaa.org/airspace-integration-flying-air-taxis-directly-into-international-airports-may-be-more-difficult-than-many-realize-experts-say/ (accessed Aug. 08, 2025).

[17] Ceren, "Airports & Air Taxis: Friends or Enemies?," Dinewithaviators, Mar. 24, 2025. https://www.dinewithaviators.com/post/airports-air-taxis-friends-or-enemies (accessed Aug. 08, 2025).

[18] Zelinski, S., "Operational Analysis of Vertiport Surface Topology," AIAA/IEEE 39th Digital Avionics Systems Conference (DASC), San Antonio, TX and Online, 11-15 Oct. 2020, DOI: 10.1109/DASC50938.2020.9256794

[19] Sheth, K., "VAMOS! A Regional Modeling and Simulation System for Vertiport Location Assessment," AIAA AVIATION 2023 Forum, San Diego, CA and Online, 12-16 June 2023, DOI: 10.2514/6.2023-3412

[20] "California's Top-performing Airport for On-time Departures Ends 2024 on a High Note — San José Mineta Intl. Airport (SJC) — Bay Area, CA," Flysanjose.com, 2024. https://www.flysanjose.com/news-release/californias-top-performing-airport-time-departures-ends-2024-high-note (accessed Aug. 08, 2025).

[21] E. Feldhoff and G. Soares Roque, "Determining infrastructure requirements for an air taxi service at Cologne Bonn Airport," CEAS Aeronautical Journal, vol. 12, no. 4, pp. 821–833, Aug. 2021, doi: https://doi.org/10.1007/s13272-021-00544-4.

[22] D. Mascio, D. Serrone, and L. Moretti, "Vertiports: The Infrastructure Backbone of Advanced Air Mobility—A Review," Eng, vol. 6, no. 5, p. 93, May 2025, doi: https://doi.org/10.3390/eng6050093.

[23] S. Lee and N. Cho, "Optimal Location of Urban Air Mobility (UAM) Vertiport Using a Three-Stage Geospatial Analysis Framework," Future Transportation, vol. 5, no. 2, p. 58, May 2025, doi: https://doi.org/10.3390/futuretransp5020058.

[24] D. Yoon, M. Jeong, J. Lee, S. Kim, and Y. Yoon, "Integrating Urban Air Mobility with Highway Infrastructure: A Strategic Approach for Vertiport Location Selection in the Seoul Metropolitan Area," arXiv.org, 2025. https://arxiv.org/abs/2502.00399

[25] "Norman Y. Mineta San José International Airport Climate, Weather By Month, Average Temperature (California, United States) - Weather Spark," Weatherspark.com, 2025. https://weatherspark.com/y/145260/Average-Weather-at-Norman-Y.-Mineta-San-Jos%C3%A9-International-Airport-California-United-States-Year-Round (accessed Aug. 08, 2025).

[26] Wikipedia Contributors, "San Jose International Airport," Wikipedia, Aug. 04, 2025.

[27] "BTS — Transtats Airports," Bts.gov, 2015. https://www.transtats.bts.gov/airports.asp?20=E&Nv42146=fWP&Nv42146_anzr=fn0%20W15r (accessed Aug. 08, 2025).

[28] "Norman Y. Mineta San Jose International Airport (SJC) — Federal Aviation Administration," Faa.gov, 2025. https://www.faa.gov/sjc?utm_source= (accessed Aug. 08, 2025).

[29] Bizjournals.com, 2025. https://www.bizjournals.com/sanjose/inno/stories/news/2023/10/12/evtol-market-analysis-venture-capital-defense.html?utm_source=chatgpt.com (accessed Aug. 08, 2025).

[30] K. R. Antcliff, M. D. Moore, and K. H. Goodrich, "Silicon Valley as an Early Adopter for On-Demand Civil VTOL Operations," 16th AIAA Aviation Technology, Integration, and Operations Conference, Jun. 2016, doi: https://doi.org/10.2514/6.2016-3466.

[31] "UBC ATSC113 crosswinds and headwinds," www.eoas.ubc.ca. https://www.eoas.ubc.ca/courses/atsc113/flying/met_concepts/02-met_concepts/02d-crosswind/index.html

[32] Federal Aviation Administration, "Aeronautical Information Manual - AIM - Controlled Airspace," Faa.gov, 2020. https://www.faa.gov/air_traffic/publications/atpubs/aim_html/chap3_section_2.html

[33] "SJC Airport Parking — San José Mineta Intl. Airport (SJC) — Bay Area, CA," Flysanjose.com, 2025. https://www.flysanjose.com/parking (accessed Aug. 07, 2025).

[34] H. V. Manuel, "Vertiport Sizing and Layout Planning through Integer Programming in the Context of Urban Air Mobility," Ub.tum.de, 2021. https://mediatum.ub.tum.de/node?id=1624149 (accessed Aug. 07, 2025).

[35] S. full bio, "Archer debuts Maker urban air taxi, first flights planned later this year," CNET, 2021. https://www.cnet.com/roadshow/news/archer-aviation-maker-urban-air-taxi-debut/ (accessed Aug. 07, 2025).

[36] Auto Futures, "'The sky is no longer the limit' – Archer Aviation to Offer 6-Minute eVTOL Flights to the Airport – CEO Adam Goldstein," Auto Futures, Jun. 28, 2022. https://www.autofutures.tv/topics/-the-sky-is-no-longer-the-limit—-archer-aviation-to-offer-6-minute-evtol-flights-to-the-airport—/s/57e93aea-44fc-44b8-9f88-84afca6c1412

[37] "What Is a Vertiport?," Archer.com, 2021. https://news.archer.com/what-is-a-vertiport (accessed Aug. 07, 2025).

[38] "Archer Flight Club: Round 5 - Safety & Certification Questions & Answers," Archer.com, 2022. https://news.archer.com/archer-flight-club-round-5-safety-certification-questions-answers (accessed Aug. 07, 2025).

[39] G. Petrauskaite, "Archer eVTOL prototype conducts first full transition flight - AeroTime," AeroTime, Dec. 02, 2022. https://www.aerotime.aero/articles/32836-archer-maker-takes-off-for-first-full-transition-flight

[40] "Archer Completes Maker's First Full Transition Flight," Archer.com, 2023. https://investors.archer.com/news/news-details/2022/Archer-Completes-Makers-First-Full-Transition-Flight/default.aspx?utm (accessed Aug. 07, 2025).

[41] Praveen, "Archer Aviation's Maker eVTOL Aircraft, US," Airport Technology, Jul. 15, 2021. https://www.airport-technology.com/projects/archer-aviations-maker-evtol-aircraft/?cf-view (accessed Aug. 07, 2025).

[42] Florin Amariei, "Stellantis-Backed Archer Presents Its eVTOL Production Aircraft Called Midnight," autoevolution, Nov. 18, 2022. https://www.autoevolution.com/news/stellantis-backed-archer-presents-its-evtol-production-aircraft-called-midnight-204176.html (accessed Aug. 07, 2025).

[43] J. Macey, "Archer Named Air Taxi Provider for LA28 Olympic & Paralympic Games - Advanced Air Mobility Intl," Advanced Air Mobility Intl, May 19, 2025. https://www.aaminternational.com/2025/05/archer-named-air-taxi-provider-for-la28-olympic-paralympic-games/ (accessed Aug. 07, 2025).

[44] Nrel.gov, 2025. https://docs.nrel.gov/docs/fy24osti/86245.pdf